Design and Analysis of Joining Methods for Open Architecture Composite Structures

by

Shane Kennedy Furlong

A thesis submitted to the Graduate Faculty of
Auburn University
in partial fulfillment of the
requirements for the Degree of
Master of Science

Auburn, Alabama
May 8, 2016

Keywords: open architecture composite structures,
tubular composite joints, joining concepts, braided composites

Approved by

Royall Broughton, Jr., Chair, Professor Emeritus of Polymer and Fiber Engineering
David Beale, Co-chair, Professor of Mechanical Engineering
Sabit Adanur, Professor of Mechanical Engineering
David Branscomb, R&D Specialist - Braids and Engineered Composites – Highland Composites

Abstract

Recent research has shown that Open-Architecture Composite Structures (O-ACS or simply Open Structures) can be utilized to create structures with characteristics that traditional composite structures cannot achieve. The stiffness to weight ratio of O-ACS exceeds comparable metal structures, as well as composite ones. The weight savings, ability to optimize, rapid manufacturability, and aesthetics provided by O-ACS components make them highly applicable to many areas. However, in order for this patented structure to complete the transition from an R&D project to a successful commercial product, a system of connecting these structures must be devised. This thesis details the design and analysis of a family of novel methods of joining O-ACS to form useful assemblies. The joining concepts can be separated at the highest level into those that are readily detachable and those that are permanently affixed. Several methods of fixturing have been examined, including; mechanical fasteners, bonding adhesives, compression fittings, and combinations thereof. A thorough investigation into design, manufacturing methods, and testing of various joining concepts has been performed and design proposals based upon the structures' constraints are put forth. Five concept joints were proposed and evaluated based on characteristics such as weight, strength, ease of manufacturing, and design utility.

The first subset of concepts investigated focuses on a component that is permanently affixed to the end of the O-ACS which allows for the structure to be mechanically fastened. One such concept consisted of a simple secondarily bonded metallic component that features a clevis for mechanical fastening of O-ACS components. This design disregards ultimate weight savings

in lieu of simplicity, allowing for efficient manufacturing and reliability. An evolution of this type of connection was developed in order to prioritize weight savings through use of a variety of composite manufacturing methods. Due to certain design criteria, a permanent joint design may be more desirable. As such, a family of coupling joints that utilize secondary bonding were developed to allow for a permanent connection between O-ACS components. Conversely, some situations require a field-deployable joint with limited resources. Therefore, a novel compression joint was designed to allow for such situations where the ability to assemble and break down an O-ACS assembly is required.

A thorough evaluation of the manufacturing processes of these joints has been conducted and testing was conducted on a range of test specimens. Test data was collected and performance is evaluated and discussed. A comprehensive design assessment on each joint is presented based on the manufacturing processes, performance, and weight.

Acknowledgements

I would like to thank Dr. Broughton for giving me the opportunity to extend my education and experiences through the O-ACS research group. The opportunity to complete my Master's allowed me to develop and mature significantly. I am very grateful for Dr. Branscomb and Highland Composites, who gave me the motivation, guidance, and resources to finish my thesis. I would also like to thank Drs. Beale, Adanur, and Foster. Thanks to the O-ACS research group; Austin, Nakul, Sanyam, Caleb, Chip, Yang, Shiv, and Uday, for all of their contributions to this work. Thank you to my loving and supportive family, without them I would not have made it here. Thank you to my Fiancé Kaitlynn for all of her encouragement and understanding.

Table of Contents

List of Figures

List of Tables

Chapter 1 – Introduction and Prior Research

This thesis focuses on the development of a novel system of joining Open-Architecture Composite structures (O-ACS). O-ACS are a braided composite structure that are inherently lattice-like and thus possess high specific stiffness and strength characteristics. Unlike many truss-like structures, O-ACS can be manufactured rapidly and in a wide variety of geometries and architectures. These structures present many unique characteristics and may be beneficial to a wide range of industries. Thus, it is apparent that a method of connecting these structures into a useful assembly is paramount. However, the non-continuous nature of the structure and thus minimal surface area, present complications when joining the structures. A brief overview of truss technology and manufacturing is given below in order to provide a comprehensive knowledge base of the structure prior to moving forward with joining methodologies.

Section 1.1 –Manufacturing of O-ACS

O-ACS are manufactured on a traditional maypole braiding machine, allowing for rapid manufacturing. The manufacturing process can be broken into 3 steps: Cord-preg manufacture, O-ACS manufacture, and curing. Cord-preg is a large cord-like yarn with an untwisted core of resin impregnated carbon fiber that is produced on a maypole braiding machine. The cord-preg is then loaded onto a larger maypole braiding machine to manufacture the O-ACS. The cord-preg is over-braided onto a mandrel, cured in an oven, and removed from the mandrel to produce the O-ACS.

Proper cord-preg manufacture is key in ensuring the manufacture of quality O-ACS. Cord-preg is made up of two components: an inner core that acts as the primary fiber reinforcement for the structure and an outer jacket that consolidates, protects, and enables further

processing of the fiber core. The core typically consists of pre-impregnated carbon fiber tows, or bundles of fibers. The core typically ranges from 12k to over 100k fibers, depending on dimensional and strength requirements. The jacket material can vary widely depending on desired aesthetics and dimensions. The jacket also contributes significantly to the overall strength of the structure by affecting the micro-joint bond, as found by Kothari [1]. The core is over-braided by the jacket in a true-triaxial geometry. The cord-pregs used in this work are discussed in further detail in the appendix (see: Cord-Preg Classifications).

Once the cord-preg has been manufactured it undergoes another braiding process to form the O-ACS. Bobbins with cord-preg are loaded onto a braiding machine in such locations that a true-triaxial braid is formed. The specifics of these locations determine the geometry of the final O-ACS. O-ACS are comprised of axial cord-pregs and helical or braider cord-pregs. The helical cord-pregs consist of a clockwise set and a matching counter-clockwise set. These cord-pregs are over-braided onto a mandrel that has been coated with release agent. The mandrel defines shape and inner diameter of the O-ACS. Traditionally the mandrel takes the form of a cylindrical metal tube. O-ACS with inner diameters of 0.375 inches up to 12.0 inches have been manufactured. One of the benefits of this unique structure is the number of parameters that can be altered: inner diameter, mandrel shape, cord-preg diameter, braid angle, number and location of axials, and number of helicals, among others. Once the O-ACS has been braided onto the mandrel, it is cured in an oven at the pre-impregnated resin's specified cure cycle. Details of the O-ACS used in the entirety of this research are discussed in further detail in the appendix (see: Standardized O-ACS).

The openness of the structure is one of its key characteristics, but also presents some challenges. The non-continuous and composite nature of the structure eliminates most of the

conventional methods of joining tubular structures. Due to the inherent lack of surface area in the structure, new joining methodologies must be devised.

Section 1.2 – Prior Research

This novel composite structure was developed by a research group at Auburn University, where it was awarded a patent [2]. Initial development and research by Branscomb laid the groundwork for manufacturing, modelling, and FEA analysis of O-ACS [3]. Cord-preg characteristics and effects on micro-joint strength were investigated by Kothari [1]. Test methods for bending and compression testing were developed by Shirgaonkar [4]. O-ACS design optimization tools were developed by Gurley [5]. Further FEA analysis and modelling contributions for both the O-ACS structure and the cord-preg were made by Shen [6].

Research on similar composite truss-like structures is scarce, although the Isotruss® that was developed at Brigham Young University shares some similarities [7] [8]. Isotruss literature makes mention of possible joining methods, such as integrally wound features, though no substantial research was uncovered [9]. NASA evaluated several composite strut designs that evaluated secondary bonding and integrally winding metal inserts to provide attachment points [10].

As such, methods of joining more traditional tubular structures were evaluated. One of the most widely used, in addition to being the most economic, system of joining prefabricated members into a truss assembly is the MERO joint [11]. The MERO joint was developed by Dr. Mengeringhausen and has provided an economic and innovative system for creating prefabricated truss structures [12]. The MERO system utilizes several node designs, among them a ball node and splice node (Figure 1 and Figure 2), to rigidly join prefabricated tubular truss members via mechanical fastening [13].

Figure 1 – MERO Ball Node

Figure 2 – MERO Splice Node

While mechanical fastening of joints in composite materials is common, adhesive bonding as the primary method of fixturing is often preferred. Benefits of adhesive bonding include reduced mass, uninterrupted fiber paths, and elimination of stress concentrations [14]. Uozumi and Kito present data on an over-braided and resin infused 4-way composite joint. The truss structure assembled with this joint was found to have superior specific strength and reduced weight compared to conventional materials [15]. Zhang investigated the joining of hybrid Aluminum-FRP truss members through the use of a novel “pre-tightned teeth connection” [16]. Although this method, along with others found, rely on a continuous tubular member with a substantial amount of surface area. Thus presents the main challenge of joining O-ACS members; inherent lack of surface area and the non-continuous nature. In summary, this literature has revealed the possibility of integrating traditional truss structure joining methodologies with the benefits of adhesive bonding when joining composite structures.

Chapter 2 – Bonded Metal Joints

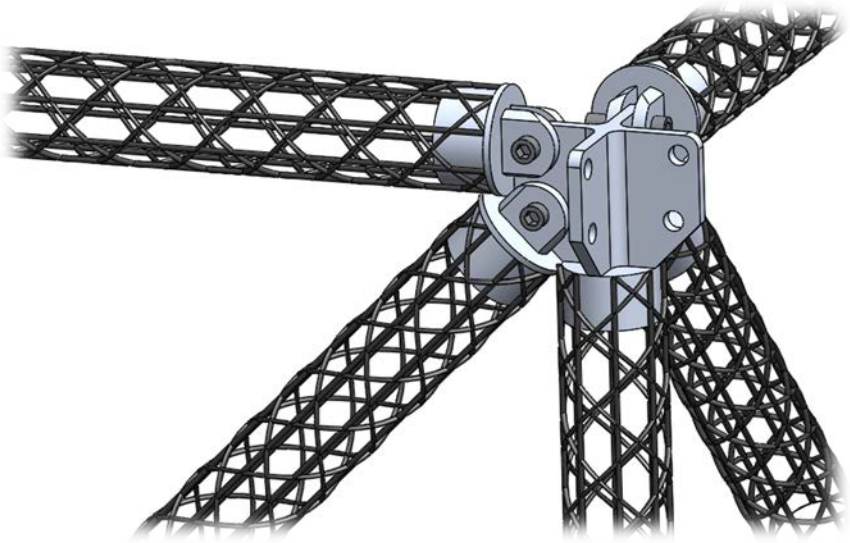

Figure 3 – Corner of O-ACS Space Frame with Bonded Metal Joints

The first method of joining O-ACS investigated was a straightforward approach that provided a method of mechanically fastening members together following the secondary bonding of an end piece into the end region. Features of this end piece can be designed in a variety of ways to account for the type of end condition desired for the given application. Elements such as threads, clevises, or various rod end attachment points can be included in the end piece design. This joining method sacrifices ultimate weight savings for simplicity and versatility. Once the O-ACS is cut to length and the joint bonded in, the member can be quickly and easily joined to other members, as depicted in Figure 3.

Section 2.1 – Design and Manufacture

A set of metal end caps were fabricated out of aluminum that included clevis features that allowed for the mechanical fastening of O-ACS. Two types of end caps were fabricated, a double clevis design (Figure 4) and a single clevis design that featured dual positions for fastening

double clevises (Figure 5). With these two designs, a unit cell of a space frame utilizing O-ACS members could be assembled and tested.

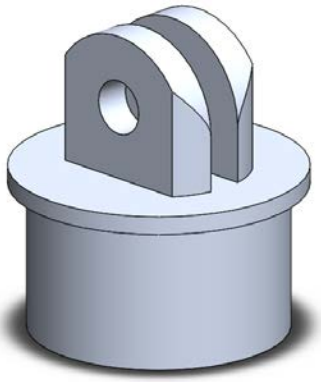

Figure 4 – Double Clevis

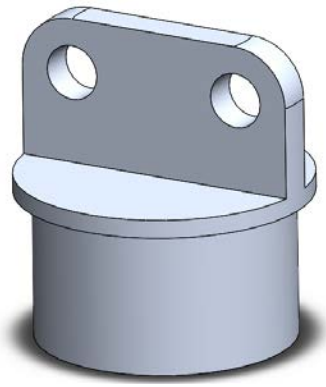

Figure 5 – Single Clevis with Dual Attachment

The bond area, the cylindrical lower portion, of these end caps were machined such that they were slightly undersized compared to the 1.75 in. diameter mandrel the O-ACS was formed on. The final outer dimension of this feature was 1.736 in. to allow for a 0.007 in. bond line gap. Surface preparation of the metal involved sanding with 220 grit followed by a solvent wipe. The adhesive used was 3M DP460 structural adhesive.

Figure 6 – Double Clevis Joint Bonded into O-ACS

These end caps were machined out of aluminum, resulting in a rather substantial amount of mass that would be added to the O-ACS. The double clevis joint had a final weight of 76.4 g and the single clevis with dual attachment points weighed 69.5 g.

Section 2.2 – Testing of Bonded Metallic Joints

Bonded metallic joints were used to create a unit cell that is representative of a space frame assembly with constituent O-ACS. To simplify testing, only two O-ACS members were used and the rest of the nodes were joined using a pinned connection. These two O-ACS members were 1 foot long and joined to the single clevis with dual attachments points to form a 70° angle. This angle was chosen based on specimen size constraints of the testing machine. Load was applied by an Intron universal testing machine to node where the O-ACS were joined, as seen in Figure 7. Compressive load was applied via constant cross head travel, at a rate of 2.5 mm/min.

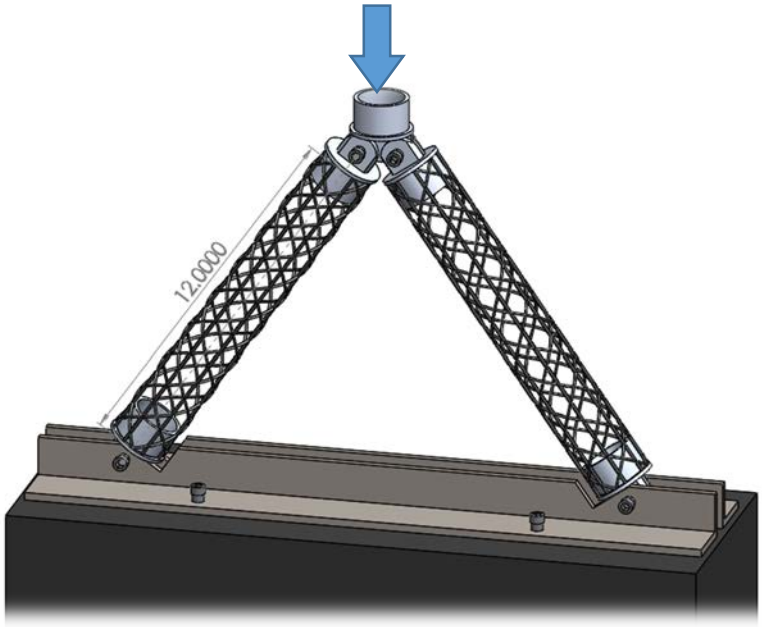

Figure 7 – Render of 2 Member O-ACS Test Specimen

Three tests were conducted on this assembly. Two of which (Test #1 and #2) involved standard O-ACS members and a third test of a standard O-ACS members with epoxy reinforced

micro-joints. The term micro-joints refers to the points within the O-ACS structure that the cord-pregs crossover each other. These micro-joints are formed by a small adhesive bond as a result of the pre-impregnated resin in the cord-preg. Due to the limited excess of resin, these joints represent a significant weak point within the O-ACS. Prior research [1] has suggested that epoxy reinforcement (3M DP 460) at these locations can substantially strengthen the structure. Figure 8 shows an O-ACS member from Test #3 with epoxy reinforced micro-joints.

Figure 8 – O-ACS with Epoxy Reinforced Micro-joints

The results of tests #1 – #3 are seen in Figure 9 below.

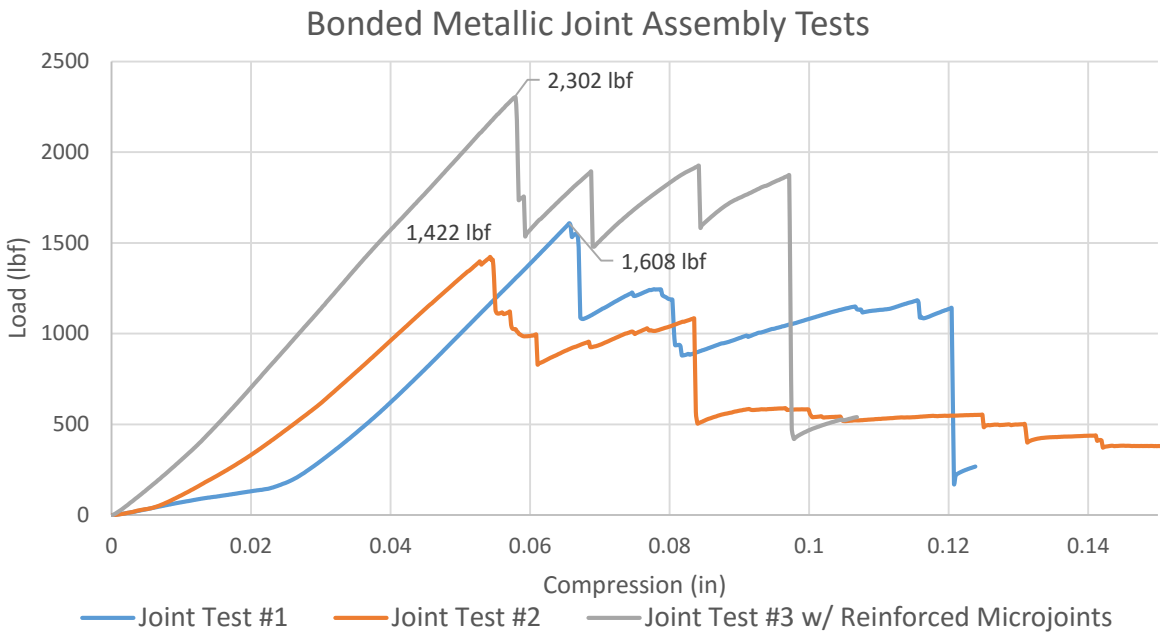

Figure 9 – Bonded Metal Joint Test Data

Section 2.3 – Discussion of Bonded Metal Joint Test Results

The above data indicated that the assemblies constructed with standard O-ACS members failed at an average of 1,515 lbf. When this peak load is resolved into the axial forces in each member, the average load per O-ACS is approximately 925 lbf. Comparatively, when standard O-ACS members were tested in pure compression failure occurred around 1,100 lbf. With only a 17.3% difference between these failure loads, it is seen that the failure occurred at 85% of the O-ACS maximum load. This reduction in strength is attributed to slight misalignments in the fixturing of the assembly, resulting in unbalanced loading. A comparison of the maximum load of the two member assembly, total load resolved into each member, and a reference test of a single O-ACS in conventional compression is shown in Figure 10.

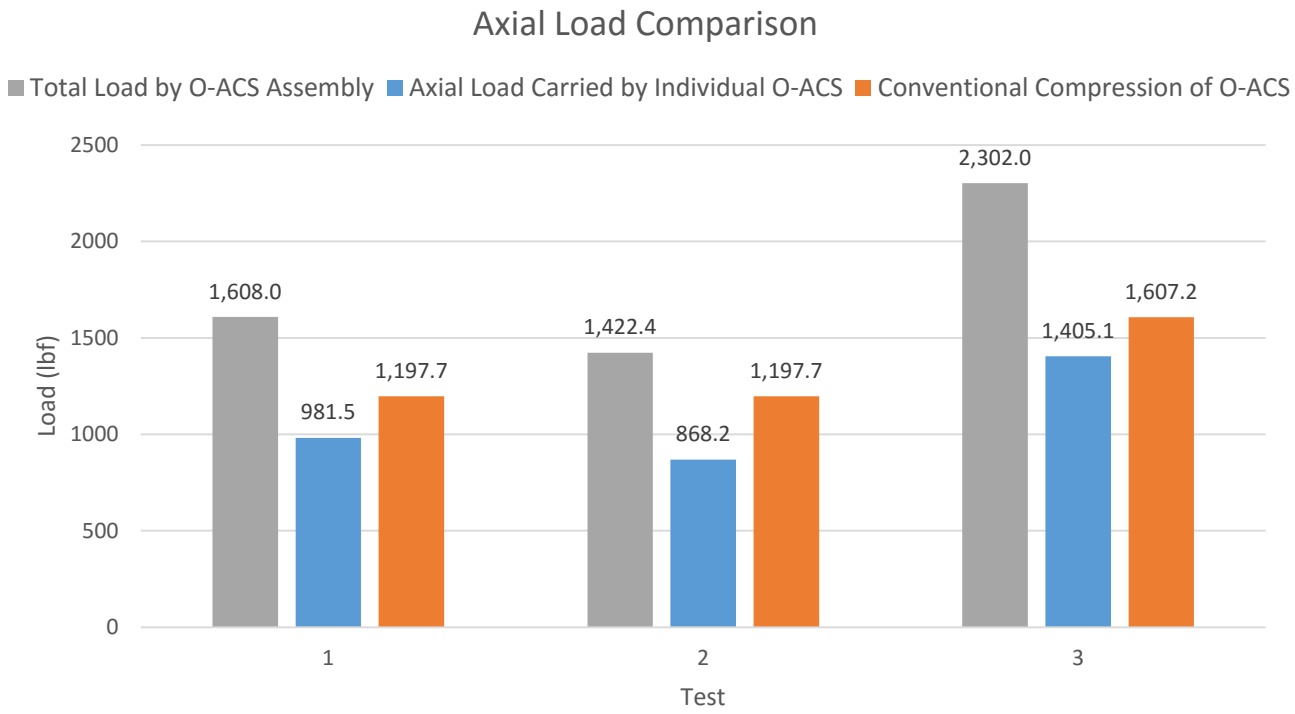

Figure 10 – Comparison of Load Carried by Assembly and Individual Structure

The resulting failures initiated in the axial components of the O-ACS, generally near the joint, as seen in Figure 11.

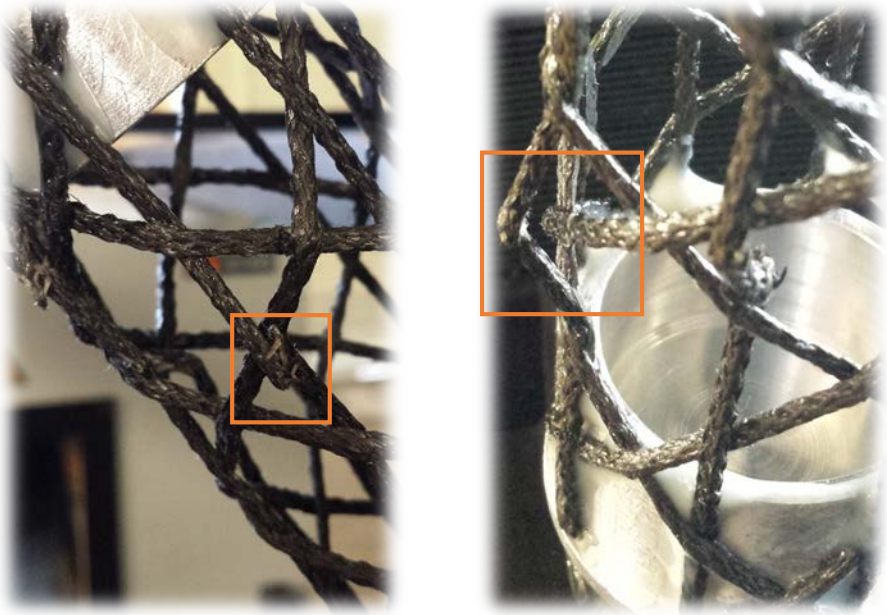

Figure 11 – Failure of Axial Cord-Pregs in Test #2

For Tests #1 and #2 there were no indications of any onset of failure in the bonded metallic joint. However, in Test #3 with the epoxy reinforced micro-joints there was a small fracture that had initiated in the epoxy prior to the failure of the axial components of the O-ACS. These failures of Test #3 are seen in Figure 12.

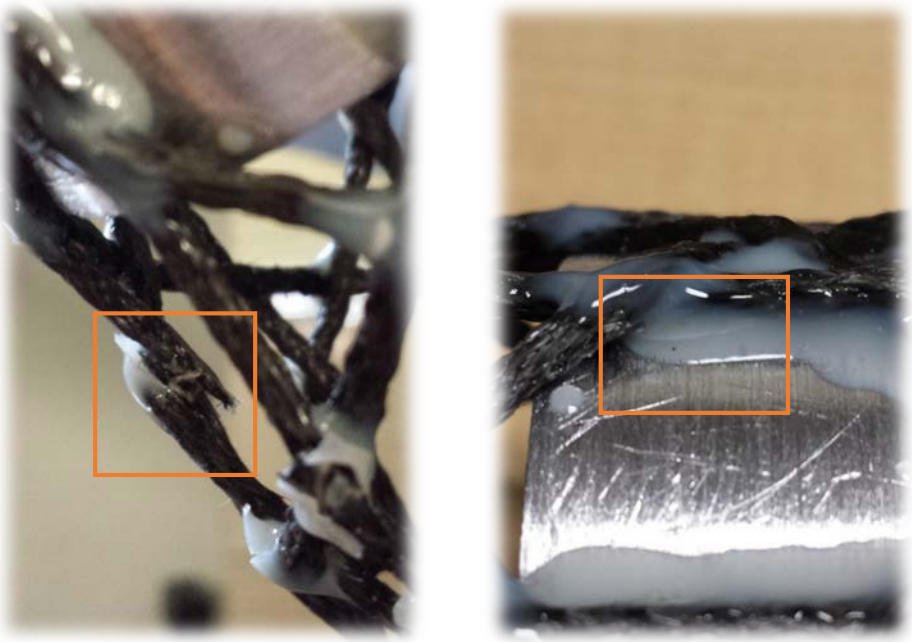

Figure 12 – Failure of O-ACS in Test #3

Section 2.4 – Characterization of Cord-Preg/Aluminum Bond

While these subassembly tests were useful in validating the concept of the joint, a more comprehensive characterization of the O-ACS/metal bond was conducted. The manufacturer of the epoxy adhesive used only provides bond strength characteristics for a small sample of substrates. While aluminum/aluminum and FRP/FRP bond strength was provided, FRP/Aluminum bond strength was not disclosed [17]. Additionally, while the cord-preg is indeed an FRP material, it has very little in common with a traditional FRP laminate. Therefore testing was conducted to characterize the cord-preg/Aluminum bond.

Testing was conducted by bonding varying lengths of cured cord-preg to an aluminum substrate. Samples of cord-preg were cured with a weight suspended from one end, insuring linearity. The aluminum substrate was prepared as the metal joints were; sanding with 220 grit sandpaper followed by a solvent wipe. Samples were prepared for three bond lengths; 0.5, 1.0, and 1.5 inches. Four samples of each length were tested in tension. Table 1 shows the resulting data from the tension tests.

Table 1 – Results of Cord-Preg/Aluminum Bond Tension Tests

1.5" Bond Length Samples

Sample	Actual Bond Length (in)	Max Load (lbf)	Approx. Shear Strength (psi)	Debond Load per unit Length (lbf/in)
1	1.522	559.66	2639.21	367.72
2	1.503	512.47	2416.67	340.97
3	1.516	781.68	3686.17	515.62
4	1.489	645.49	3043.96	433.51

1.0" Bond Length Samples

Sample	Actual Bond Length (in)	Max Load (lbf)	Approx. Shear Strength (psi)	Debond Load per unit Length (lbf/in)
1	1.02	470.69	3329.45	461.46
2	0.996	512.33	3623.98	514.39
3	1.001	550.64	3894.97	550.09
4	0.974	483.72	3421.62	496.63

0.5" Bond Length Samples

Sample	Actual Bond Length (in)	Max Load (lbf)	Approx. Shear Strength (psi)	Debond Load per unit Length (lbf/in)
1	0.508	290.00	4102.62	570.86
2	0.497	297.49	4208.66	598.58
3	0.495	296.61	4196.21	599.22
4	0.509	311.80	4411.09	612.58

An approximation of the shear strength of the bond is calculated based on half the surface area of a cylinder. This approximation is discussed in greater detail in Section 4.4.1, Equation 3. Because of the difficulty in defining diameter and accurately calculating bond surface area of cord-preg, load per unit length is calculated. The average debond load, in tension, per unit length was found to be 505.13 lbf/in of bond length for cord-preg #6/Aluminum substrates bonded with

3M DP460. By characterizing the bond strength per unit length as opposed to calculated approximate surface area, a more straightforward approach to designing a bonded metallic joint is achieved. The total length of cord-preg in the bond region on any O-ACS geometry can be approximated using Equation 1.

$$Total\ Length\ of\ Bond\ Area = (L * A) + \left(H * \frac{L}{cos\theta}\right)$$

$L = Length\ Bond\ Area$
$A = \#\ of\ Axials$
$H = \#\ of\ Helicals$
$\theta = Braid\ Angle$

Equation 1

A spreadsheet was generated that, following the input of O-ACS geometry and bond strength per unit of bonded length, allows for calculation of debond load of the O-ACS and metallic joint. Table 2 shows the calculation for the standard O-ACS and bond length of 1 inch; a maximum load of 11,733.64 lbf in tension is calculated.

Table 2 – Bond Failure Calculation for Standard O-ACS

Joint Bond Length (in):	1.00
# of Axials	8
# of Helicals	8
Braid Angle (θ)	45.0
Debond Load per Length (lbf/in)	505.13
Total length of bond area (in):	23.23
Structure Load to Bond Failure (lbf):	11,733.64

Using this method of bond characterization, the optimum bond length of the joint can be calculated, based on the load the joint is expected to sustain. By minimizing this bond length, the overall weight of the bonded joint can be greatly reduced. Methods of further reducing the weight by maximizing the bond surface area are discussed in Section 4.2.

Section 2.5 – Conclusions from Evaluation of Bonded Metallic Joints

This chapter investigated the characteristics of a simple and predictable method of connecting O-ACS. This joining method relies on secondary bonding of an external structure into the end of the O-ACS that has one or more features that allow for a method of connection. The joint designed and manufactured in this section included a clevis feature to allow for mechanical fastening to other structures. A unit cell of a truss-structure that utilized O-ACS as the members was assembled and tested. The O-ACS members sustained a load of comparable magnitude as a comparable structure loaded in simple compression, showing there was minimal loss of strength in the O-ACS as a result of joint design. The positive effect of epoxy-reinforced micro-joints was also demonstrated. The bond between the cord-preg and aluminum joint was characterized in pounds per unit length such that bond length of the joint may be optimized for any O-ACS. This allows for joint strength to match O-ACS strength such that unessential mass is not added. Assuming the tensile failure load of a standard O-ACS is approximately 5,500 lbf, as seen in Section 4.3.2, a bond length of 0.5 inches would provide a bond that exceeds the maximum tensile load of the O-ACS.

While this joining method provides predictability, simplicity, and a variety of connection types; it is not without disadvantages. The mass added by bonding a metal joint into an O-ACS is substantial. However, by optimizing the bond length and integrating features to maximize bond area, mass can be removed. Aluminum was chosen for ease of manufacture and availability. However, this type of joint could be rapidly manufactured via plastic injection molding. By producing this style joint by plastic injection molding of high strength thermoplastic such as glass filled nylon, high levels of production could be attained while minimizing weight and maintaining appreciable strength.

Chapter 3 – Tapered Joint with Metallic Insert

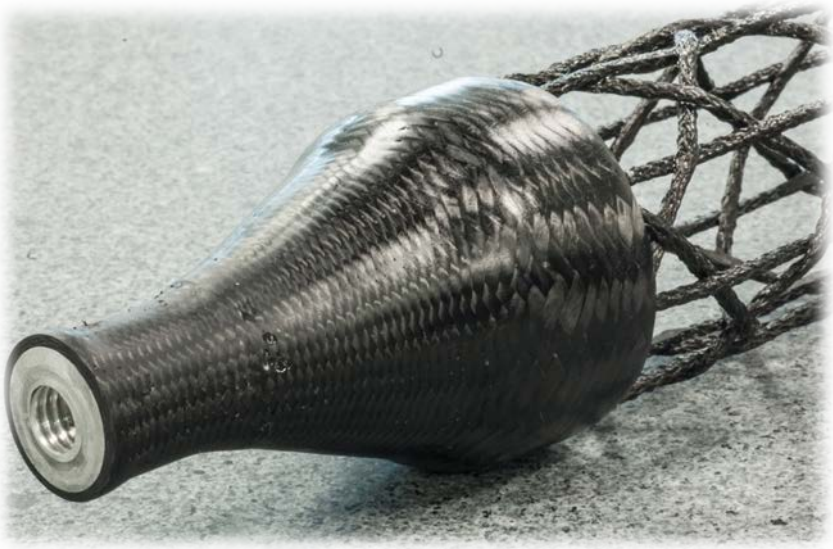

Figure 13 – Over-Braided Joint with Metallic Insert

This chapter investigates three possible manufacturing methods for a tapered composite joint that is secondarily bonded to the end of an O-ACS. This composite joint features an integral metallic insert with internal threads that can provide a versatile means of connecting O-ACS, as seen in Figure 13. Prototypes are manufactured via filament winding, hand lay-up, and over-braiding processes. Additionally, several insert designs and integration methods are evaluated. Testing is conducted to determine failure loads and a thorough assessment of the varying manufacturing methods is presented.

A method of connecting O-ACS that allows for disassembly, a variety of connection methods, and excellent strength characteristics would provide a suitable connection for a wide range of O-ACS applications. Based on an evaluation of existing methods of creating space frames and connecting tubular members, a method of integrating threads into the O-ACS was pursued. The incorporation of threads into an O-ACS provides a proven and universal method of connecting structural members to form a wide range of assemblies. An O-ACS with threads can be outfitted with a variety of rod-ends. Rod-ends such as a clevis would provide a pinned end

condition; depicted in Figure 14 and Figure 15. Figure 16 and Figure 17 show a method of creating a fixed end condition via a spherical node joint that is used to create large space frame structures using tubular strut members. This gives the O-ACS joint the ability to be assembled and disassembled; as well as providing a mechanism to finely adjust overall length between connection points. Additionally, because of the universal nature of threaded connections, machining custom connections to meet customer demands would be trivial.

Figure 14 – Rod End

Figure 15 – Double Clevis Rod End

Figure 16 – Spherical Node Joint

Figure 17 – Truss Structure with Spherical Node Joints

Section 3.1 – Design and Manufacture

Due to the brittle nature of composites, it is typical to introduce a metallic insert or bushing to allow for threads or mechanical fastening. This provides a way to evenly distribute loads to the reinforcing fibers. To compensate for the introduction of a discontinuity in the fibers and matrix, adhesive is introduced to bond the insert into the composite laminate. Therefore, a method of integrating a metallic insert with a threaded internal bore into the O-ACS end region was designed. Because the typical O-ACS diameter is much larger than the required thread size,

a tapered region must be incorporated into the design. In order to minimize the amount of mass added to the O-ACS, a carbon fiber-epoxy composite material was chosen. Several methods of manufacture were evaluated: Filament winding, hand lay-up, and over-braiding. Prototype joints were manufactured with each of these processes and assessed. Additionally, the design of the metallic insert was investigated. Many traditional inserts rely on secondary adhesive bonding for integration; but, methods such as filament winding and over-braiding provide an additional mechanical locking of the insert provided a suitable design.

Section 3.2 – Filament Winding

The first process investigated was filament winding over a water soluble wash-out mandrel. The filament winding process lends itself well to the manufacture of such a joint due to the cylindrical shape of the joint and ability for rapid manufacture. However, several drawbacks were encountered. The Durawound Cobra filament winder used was not CNC controlled and did not have a suitable tensioning device, leading to difficulties traversing the taper and severe limitation of the winding angle. As a result, a lay-up schedule consisting of filament wound 90° (hoop wrapping) tow-preg plies and 0° unidirectional pre-preg was chosen.

Figure 18 – V-Groove and Double Taper-In Metal Inserts

Two metal insert designs were evaluated, as seen in Figure 18. The grooved and tapered regions of the inserts were designed to trap and allow a built up region of filament wound tow-preg to provide a mechanical locking effect, in addition to the adhesive bond with the epoxy.

A wash-out mandrel was fabricated using a 3D printed mold to facilitate easy removal of the mandrel (Figure 19). The mandrel was initially created with gypsum plaster, as seen in Figure 20, but improved mandrels were fabricated with a water soluble ceramic (AquaCore manufactured by ACM) material and then machined to the desired dimensions.

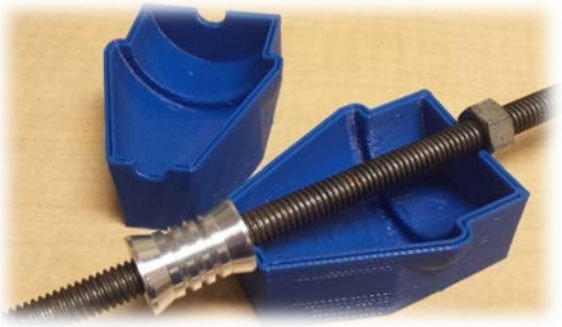

Figure 19 – 3D Printed Mold and Metal Insert

Figure 20 – Gypsum Plaster Mandrel and Insert

Figure 21 – Filament Winding of 90° Ply #1

Table 3 – Lay-up Schedule	
Ply Number	**Direction**
1	90°
2	0°
3	0°
4	0°
5	90°
6	0°
7	0°
8	0°

Figure 21 shows the filament winding of tow-preg for ply #1. The tension and traverse rate of the eyelet was controlled by hand due to the limitations of the filament winder. Table 3

details the lay-up schedule for the joints; with 90° referring to a filament wound ply and 0° consisting of unidirectional pre-preg material.

Section 3.3 – Hand Lay-up

The second method of manufacturing the joint was performed by hand lay-up with braided carbon fiber sleeve. Joints manufactured with this method saw an evolution in design carried over from the composite coupler joint, discussed in Section 4.2; the annular channel to increase bonding area. This channel, seen in Figure 33, provides greater than two times the amount of bonding area by encapsulating the entire end region of the O-ACS in carbon and bonding adhesive. An aluminum mandrel was machined to the proper dimension to provide integration of a standard O-ACS. Highland Composite 1.75 in. carbon fiber braided sleeve was laid up of the mandrel along with a silicone ring, similar to the manufacturing method of the

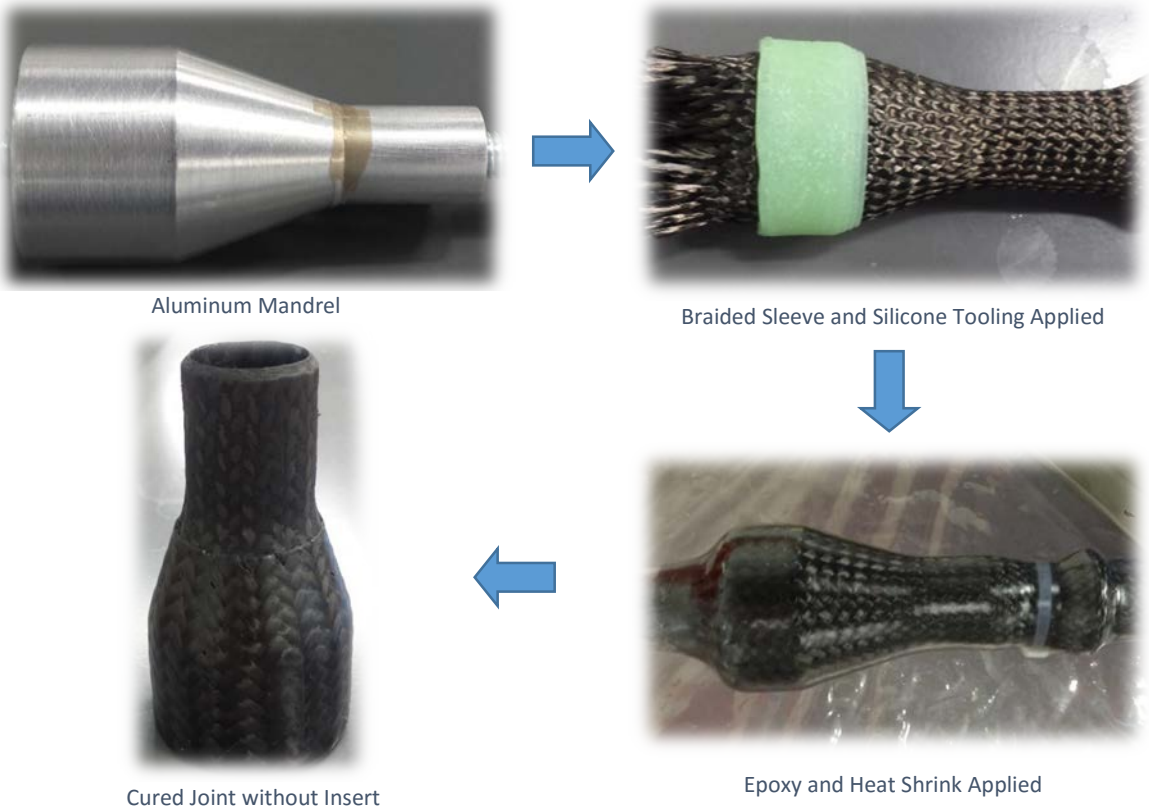

Figure 22 – Hand Lay-up Process

composite coupler. Araldite LY 8601 epoxy was used to wet out the braid and heat shrink tubing was used to provide compression and improve the surface quality. This process is illustrated in Figure 22.

However, it was deemed that the heat shrink tubing provided inadequate compaction to provide a substantial mechanical locking effect on the metal insert. As such, the insert for hand laid-up joints were secondary bonded into the cured joint. This process was achieved by machining a cylinder that would fit into the narrow end of the taper that was 1 inch in length with internal threads. This insert was then media blasted and bonded in place with 3M DP460 structural epoxy. The insert was machined to allow for a 0.007 inch thick adhesive bond thickness.

Section 3.4 – Over-braiding

The last process investigated for the manufacture of this joint was over-braiding. Over-braiding is a process of braiding over a form or mandrel which allows for a very tight and well compacted fiber preform. This type of method would typically be followed by some variation of liquid resin infusion process (RTM or VARTM), but due to the simplicity of the part, hand wet-out was chosen in conjunction with shrink tube to provide improved surface finish. This approach utilized the evolutions and lessons learned from the prior methods; a ceramic wash-out mandrel to ease mandrel extraction, silicone tooling to create an annular channel for improved bonding, and re-designed metal inserts optimized to the over-braiding process.

Three designs for the metallic insert were evaluated (Figure 23 – Figure 25). The first design was carried over from the filament winding design, but was not as well designed to create a mechanical lock from the fiber paths created by the over-braiding process. While the V-grooves in Figure 23 effectively trap filament wound fiber paths, the fiber paths created by over-

braiding do not lock into the V-grooves. The helical fiber paths created by the braiding process do not lay down into the grooves like a filament wound tow does. Therefore, a taper design that incorporates cross-section area transitions was created to take advantage of the ability of the braid to change diameter. The double taper-in design was inverted to provide a larger diameter that was within the braiding machines lower limit; referred to as the double taper-out design. Additionally, a quad-taper design with pins was fabricated. The pin elements are loaded in shear as the fibers bear against them in during loading. These designs were evaluated against each other to determine the importance of the mechanical locking effect.

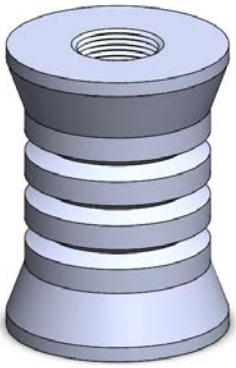

Figure 23 – V-Groove Design

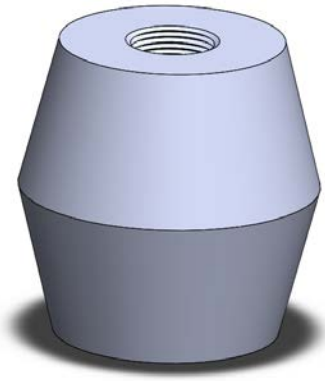

Figure 24 – Double Taper-Out

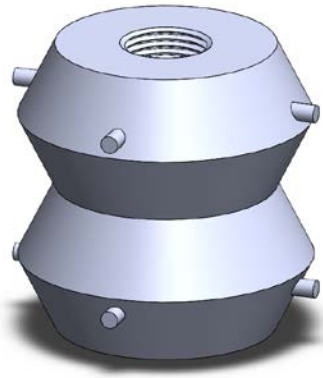

Figure 25 – Quad-Taper with Shear Pins

As in the previously described processes, a ceramic wash-out mandrel was machined to the desired dimensions on a threaded rod. This mandrel was then covered in Teflon© tape to prevent resin ingress during cure. Figure 26 shows the quad-taper insert and wash-out mandrel without Teflon© tape.

Figure 26 – Wash-out Mandrel and Metal Insert Assembled

The over-braiding process was carried out using a EuroCarbon 64 carrier braiding machine. This machine was selected for its ability to over-braid small diameter mandrels. The machine was loaded to full capacity (64 bobbins) that were wound with Hexcel 6k AS4C Carbon fiber. An initial layer of carbon was over-braided, after which the silicone tooling was inserted into the pre-form. Two more over-braiding passes were performed to provide full coverage of the mandrel and provide the desired strength. This process is illustrated in Figure 27 through Figure 32.

Figure 27 – Mandrel mounted for over-braiding

Figure 28 – Over-braiding of First Layer

Figure 29 – Layer 1 Complete and Insertion of Silicone Tooling

Figure 30 – Final 2 Layers Over-braided

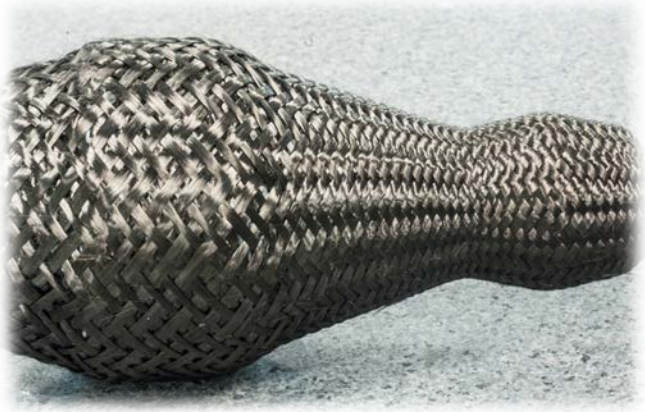

Figure 31 – Double Taper-Out Preform

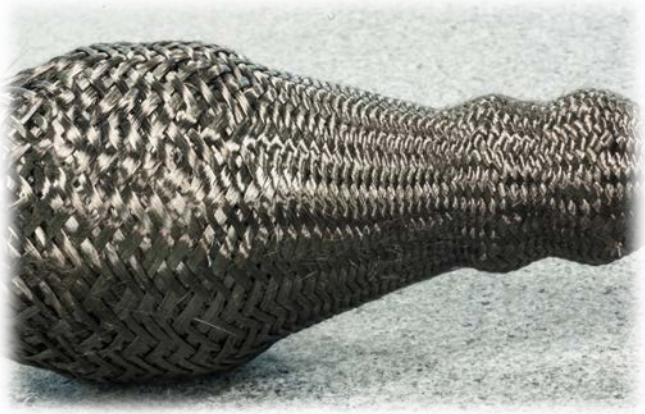

Figure 32 – Quad-Taper with Preform

Upon completion of the over-braiding process, the preform was wet-out with Araldite LY 8601 epoxy resin and encapsulated in shrink tube. It was cured at 175° F for 1 hour to accelerate the curing process. After which the shrink tube was cut away and the ceramic mandrel was washed out with water. The threaded rod was removed and the composite part was trimmed to allow for removal of the silicone tooling. The finished joints are shown in Figure 33 through Figure 36.

Figure 33 – Annular Channel Detail

Figure 34 – Joint with V-Groove Insert

Figure 35 – Joint with Double Taper-Out Insert

Figure 36 – Joint with Quad-Taper Insert

Section 3.5 – Compression Testing of Tapered Joints with Metal Inserts

Eight joints with metallic inserts were manufactured and tested in compression. As discussed in the previous sections, three manufacturing processes and four insert designs were evaluated. Furthermore, several methods of integrating the insert were assessed; secondary bonding, mechanical locking, and film adhesives. Compressive loading was chosen to simplify fixturing methods, as well as indicating whether the insert had failed or the composite. Additionally, the joint is expected to fail under compression significantly earlier than when loaded in tension. Two areas of failure were of interest; the load needed to dislodge the insert from the composite joint and the onset of failure in the composite.

Fixturing was achieved by potting the base, the region which would be bonded onto the O-ACS, in epoxy resin. Bonding the joints to O-ACS for testing, as they would be in normal use, was avoided in order to determine failure modes of the joints and exclude any premature failures induced by the failing O-ACS. Perpendicularity between the centerline of the threads and the base of the resin ‘puck’ was ensured by suspending the joint in the uncured resin, similar to suspending a plumb bob. This effectively constrained the base of the composite, eliminating the possibility of premature failure in the event of the unsupported base ‘end brooming’. The resin encapsulated base was placed on the cross-head of the Instron 4505 universal testing machine. A bolt was threaded into the metal insert, providing a secure point of contact for the load cell. This effectively transferred load from the threads of the inserts and into the composite joint. The resin potting provided similar constraining conditions as the joint would experience when bonded into an O-ACS. Figure 37 shows over-braided joint sample #5 potted in epoxy and fixtured in the Instron.

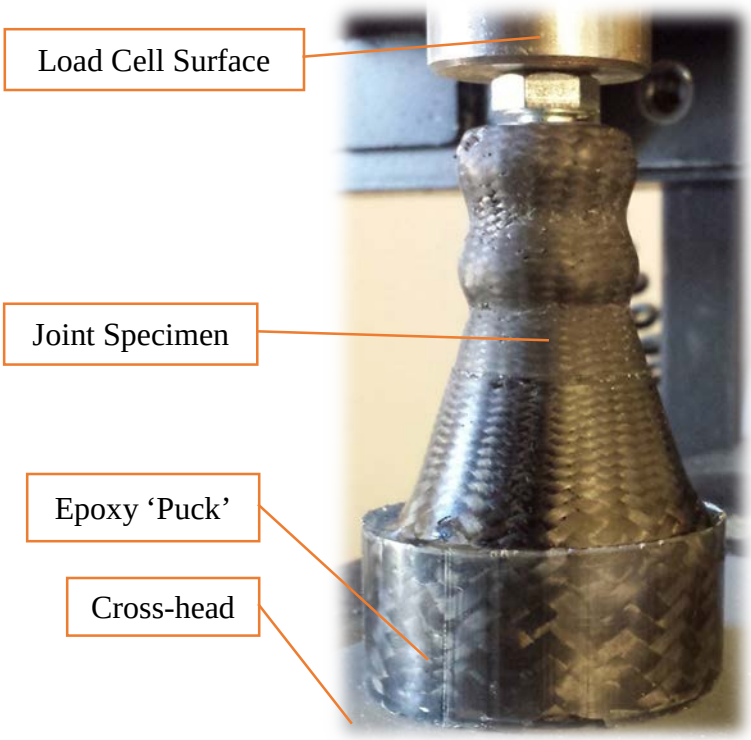

Figure 37 – Over-Braided Joint Sample #5 Ready for Testing

Test procedures were based off of ASTM D3039 Standard Test Method for Tensile Properties of Polymer Matrix Composite Materials, as no comparable standard for compression was found. Constant crosshead travel was chosen due to the inability to measure strain in situ and unknown compliances within the method of fixturing. Cross-head speed was set for 2 mm/minute. This fixturing method and test method was used for all composite taper joints with metal inserts.

Section 3.5.1 – Testing of Filament Wound Taper Joints

Three joints that were manufactured via a filament winding process were evaluated. Two insert designs and two methods of integrating the insert were tested. All were tested in compression in the fashion described in Section 3.5. The methods of manufacturing the three test samples are discussed below.

Filament wound joint #1 was manufactured with a V-groove style insert, as seen in Figure 23. The method of integration was mechanical locking supplied by the filament wound fiber tows. Additionally, the pre-impregnated resin served as a supplemental adhesive bond.

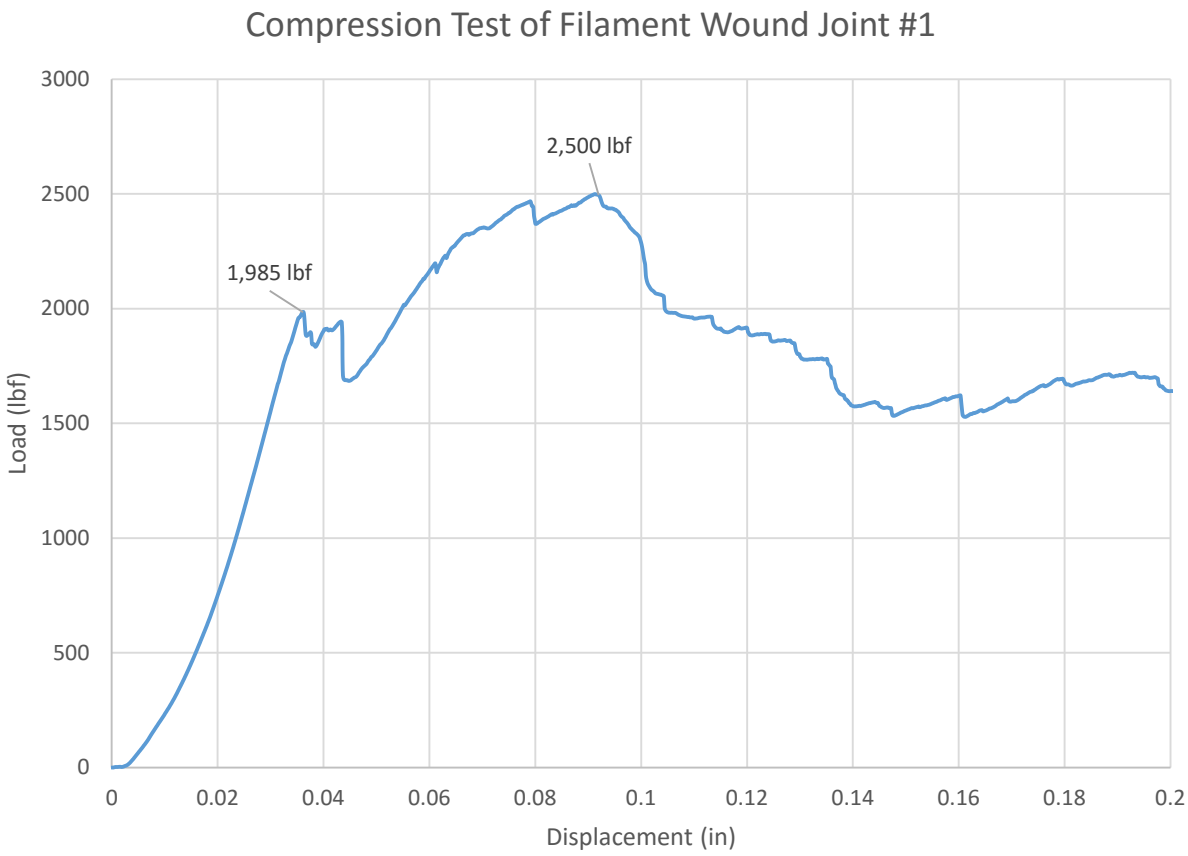

Figure 38 – Load vs. Displacement for Filament Wound Joint #1

Filament wound Joint #1 failed in two stages. The first, more abrupt failure at 1,985 lbf was the insert dislodging inside the composite. However, the insert did not fail catastrophically, after shifting approximately 0.040 inches in the direction of the applied load, the insert became locked in place. It is inferred that this failure is representative of an adhesive failure between the resin system and the insert. After a slight repositioning, the fibers that interlock into the grooves of the insert take up the load. After reaching a

peak load of 2,500 lbf, the composite failed near the end of the taper region. The slight repositioning of the insert and failure of the composite is seen in Figure 39.

Figure 39 – Failure of Filament Wound Joint #1

Filament wound joint #2 was manufactured with a double taper-in design, as seen on the right side of Figure 18. The method of integration was mechanical locking supplied by the filament wound fiber tows. Additionally, the pre-impregnated resin served as a supplemental adhesive bond as previously mentioned. Figure 40 shows the load vs. displacement on the joint.

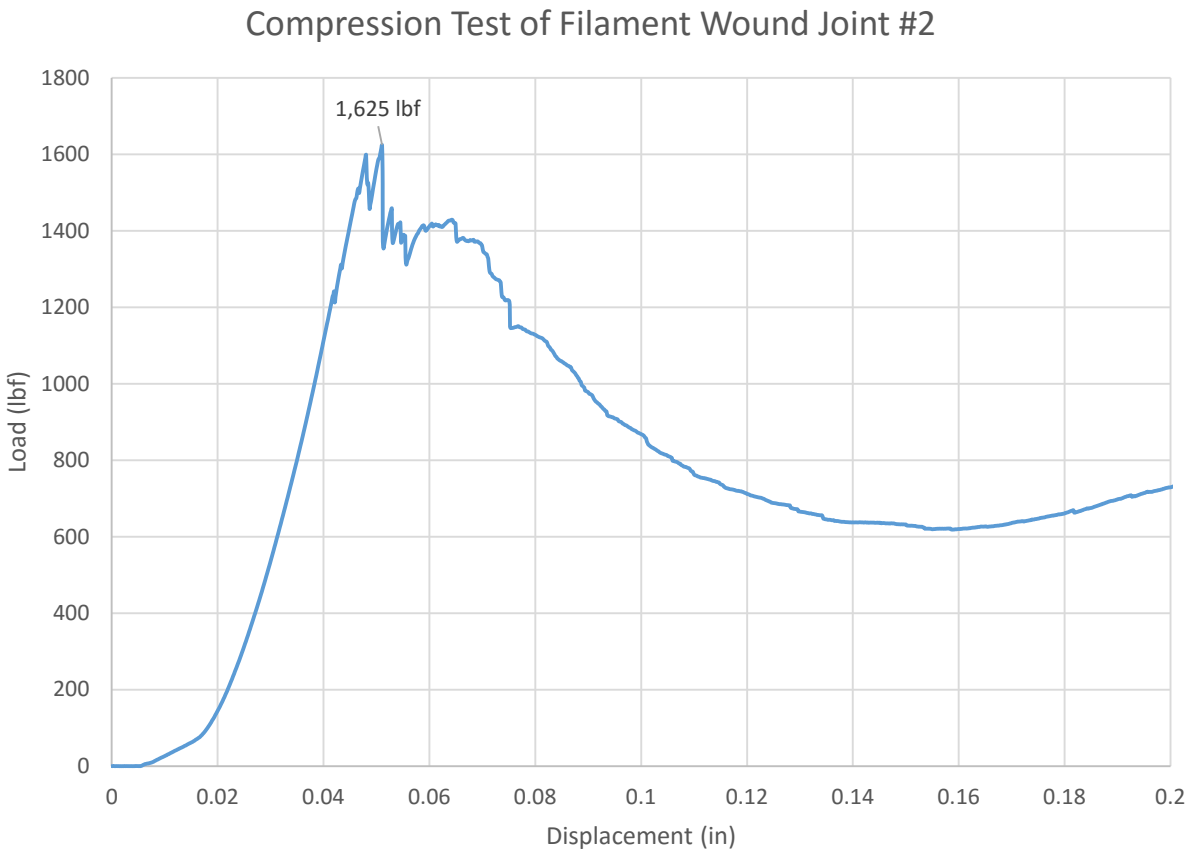

Figure 40 – Load vs Displacement of Filament Wound Joint #2

Filament wound joint #2 failed in the region near the end of the taper, similar to the secondary failure of filament wound joint #1. However, there was no noticeable dislodging or repositioning of the insert within the composite. A peak load of 1,625 lbf was reached, although onset of failure began at 1,599 lbf. The failure of the composite is seen in Figure 41.

Figure 41 – Failure of Filament Wound Joint #2

Filament wound joint #3 was manufactured with a double taper-in insert, identical to filament wound joint #2. This joint differs from the previous by the addition of a film adhesive applied to the metal insert prior to winding of ply #1. Therefore this insert was integrated via a substantial adhesive bond, in addition to the mechanical locking provided by the insert design. Figure 42 shows the load vs. displacement on the joint.

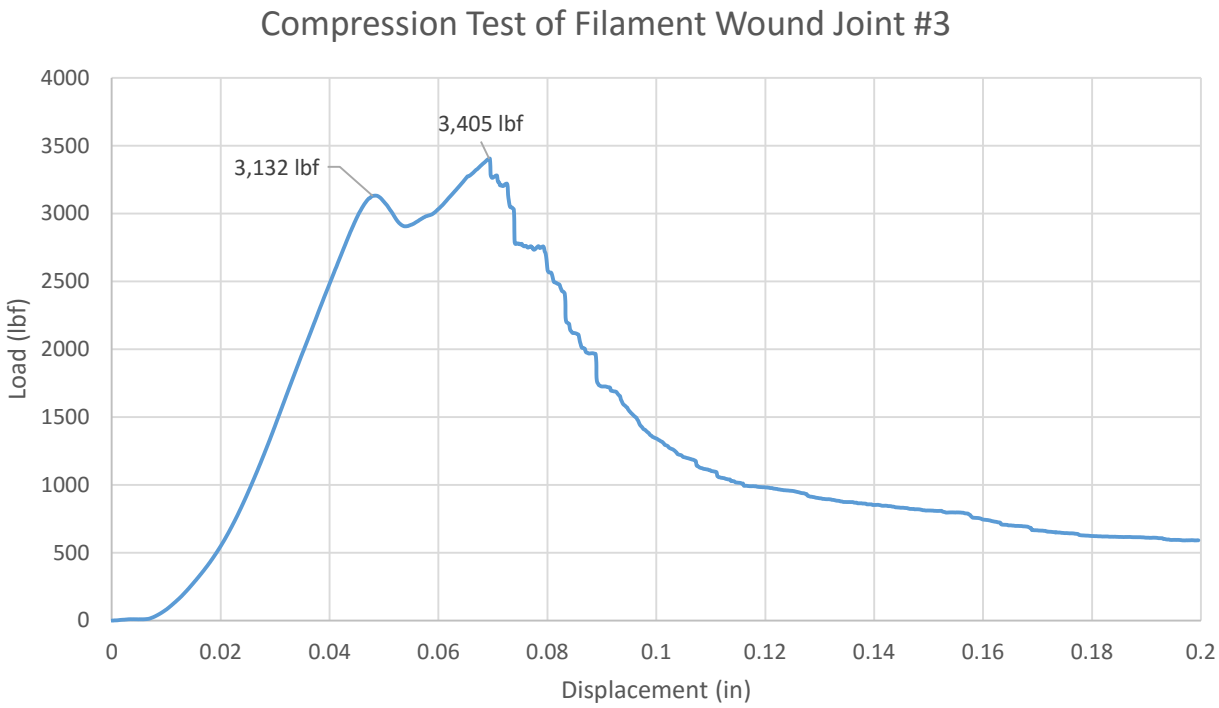

Figure 42 – Load vs. Displacement for Filament Wound Joint #3

Filament wound joint #3 failed in similar fashion as filament wound joint #1, in that there were two stages of failure. An initial debonding and dislodging of the insert, followed by a crushing of the composite in the end region of the taper. This initial adhesive failure occurred at a load of 3,132 lbf when the insert was dislodged by approximately 0.020 inches. After this failure, it is suggested that the fibers occupying the narrow tapered area picked up the load, allowing for a continued rise in load. After reaching a peak load of 3,405 lbf the composite failed near the termination of the taper, as seen in Figure 43.

Figure 43 – Failure of Filament Wound Joint #3

Section 3.5.2 – Testing of Hand Lay-up Joints

One joint was fabricated via the hand lay-up process. Due limitations discussed in Section 3.3, the insert in this joint was secondarily bonded into the joint. As such, there was no mechanical locking effect and the insert relied solely on the adhesive bond. Figure 44 shows the load vs. displacement for the hand laid-up joint.

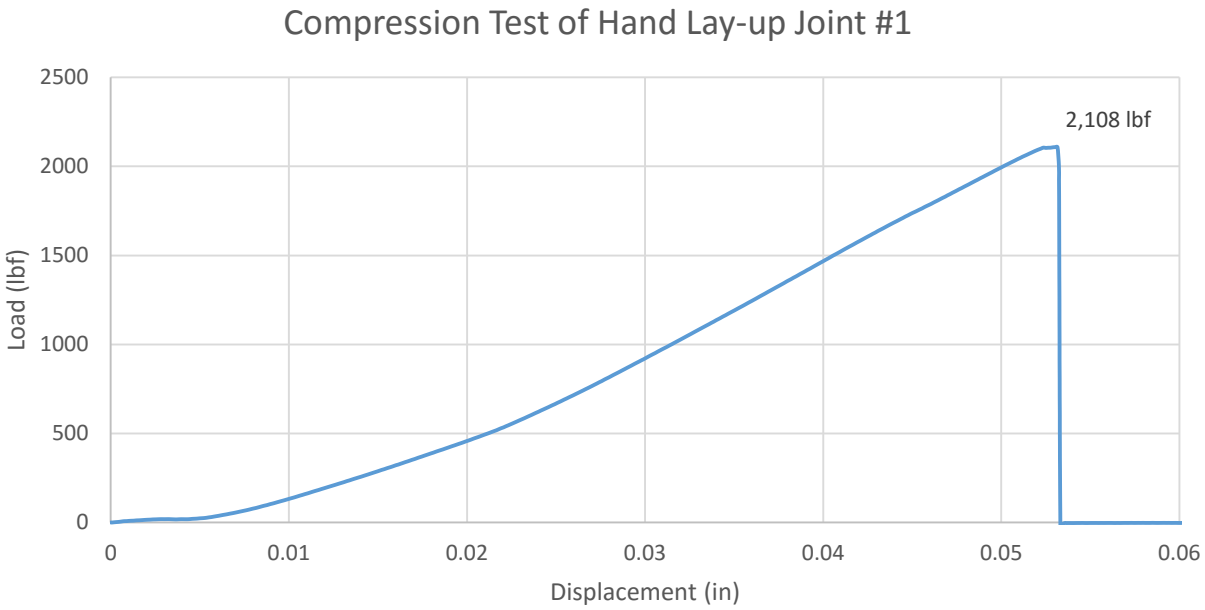

Figure 44 – Load vs Displacement for Hand Laid-up Joint #1

This data clearly shows an abrupt adhesive failure between the insert and the composite. The secondary bond that retained the metal insert failed at a load of 2,108 lbf. After the adhesive failure, there was no mechanical locking provided by this insert design; resulting in the inability for the joint to further sustain any load.

Section 3.5.3 – Testing of Over-braided Joints

Four joints were fabricated through the process of over-braiding. Each joint was formed with a different metallic insert design. All inserts relied primarily on a mechanical locking between the fibers and the contour of the metal insert. A subsequent adhesive bond was also present between the insert and the epoxy matrix. The details of the manufacturing method of each sample are provided subsequently.

Over-braided joint #1 was manufactured with a double taper-in insert, seen in Figure 18. This joint was over-braided in a different manner than all the subsequent joints. Joint #1 was over-braided with the 64 carrier EuroCarbon braiding machine loaded at half capacity; 32 bobbins. This results in a diamond braid architecture, where the fibers braid 1/1 repeating pattern, or ‘1 over, 1 under’ fashion. While a normal biaxial braid uses a 2/2 repeating pattern. The mandrel was over-braided with two layers of a 32 end diamond braid. Compared to over-braided joints #2 – #4, which were over-braided with 3 layers of 64 end conventional braid, joint #1 had one third the amount of carbon fiber reinforcement. The load vs displacement data is presented in Figure 45.

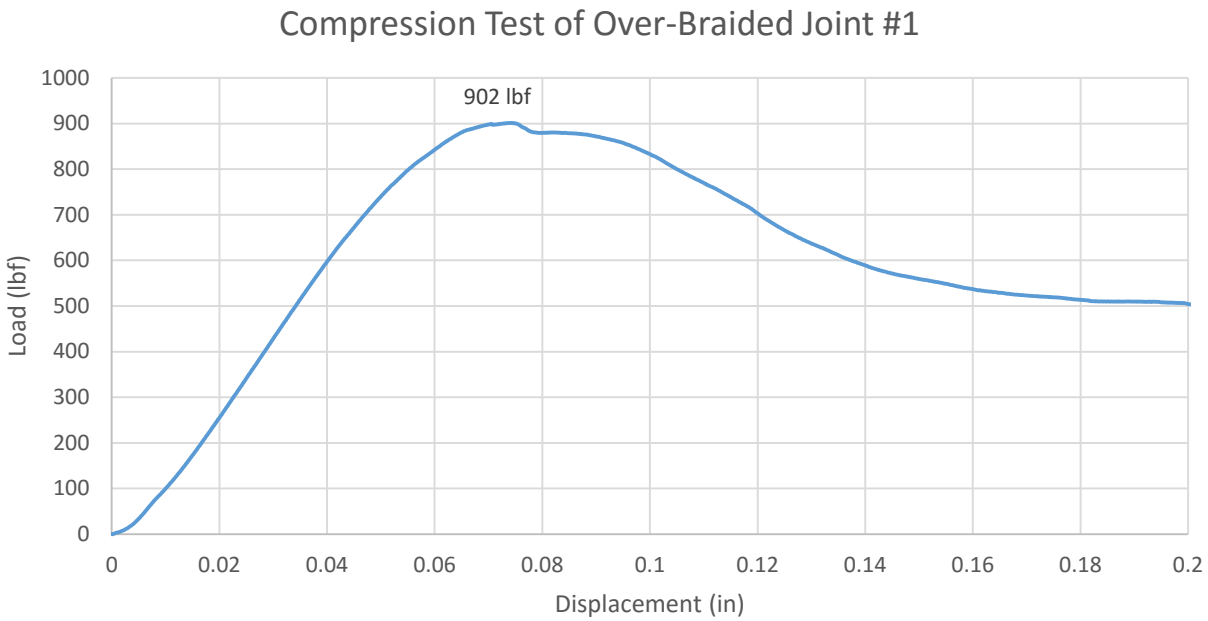

Figure 45 – Load vs Displacement for Over-Braided Joint #1

This joint sample exhibited no signs of insert debonding or shifting. The failure of the joint occurred in the composite, nearest the potted region. This onset of failure in the composite initiated at 902 lbf. The failed joint is shown in Figure 46.

Figure 46 – Failure of Over-Braided Joint #1

Over-braided joint #2 was manufactured with a V-groove insert, the same as filament wound joint #1. This insert design is seen in Figure 23. While this V-groove design does not effectively trap fibers from the over-braiding process, it was chosen to compare the over-braiding process to that of filament winding. Figure 47 presents the load vs displacement data for over-braided joint #2.

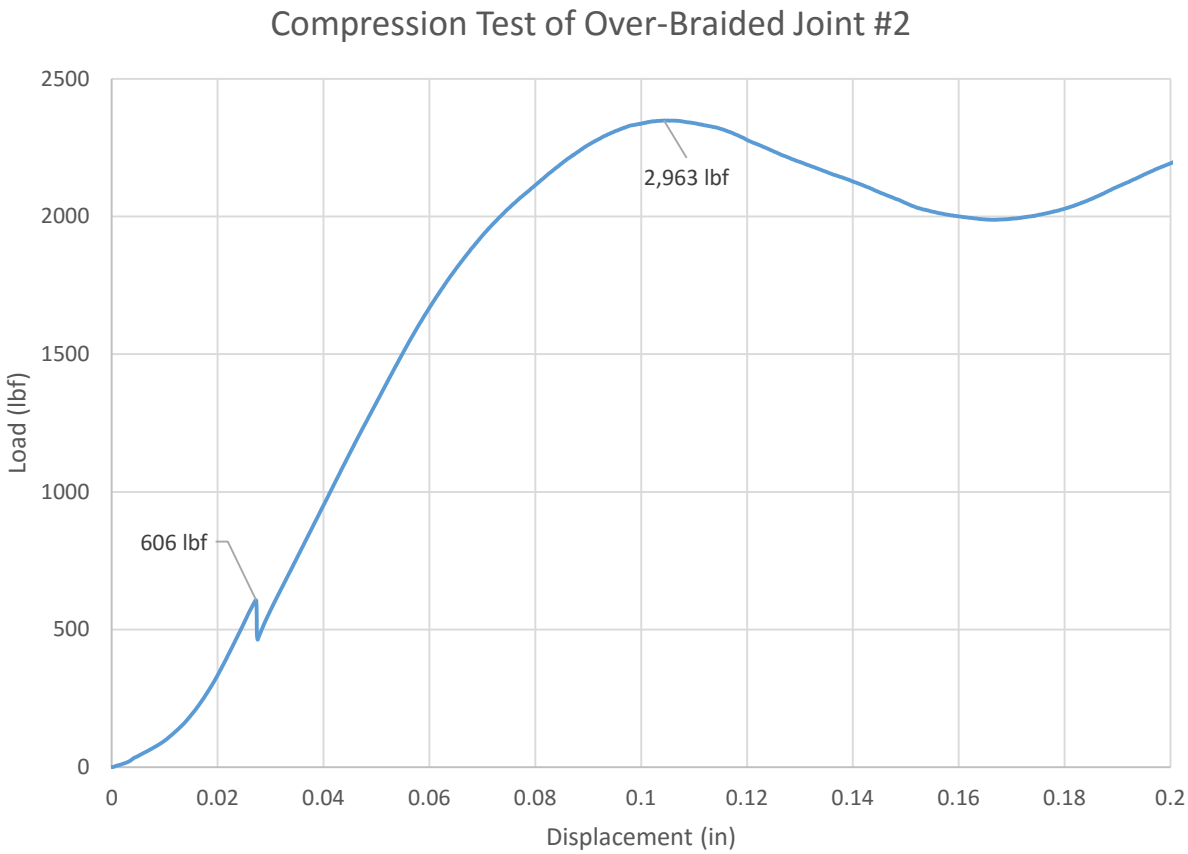

Figure 47 – Load vs Displacement for Over-Braided Joint #2

This joint failed by an initial debonding of the insert, at a load of 606 lbf. After this debonding, the insert was forced downwards into the composite. The insert was dislodged a distance of 0.125 inches. Due to the slight tapers at the edge of the insert, the insert was not entirely free to slide, allowing for a continued loading of the joint. The joint continued to withstand loading, which eventually led to a failure of the composite at

a peak load of 2,963 lbf. The failure occurred in the taper region of the composite, nearest the edge of insert, as seen in Figure 48.

Figure 48 – Failure of Over-Braided Joint #2

Over-braided joint #3 incorporated an insert with the double taper-out design, as seen in Figure 24. This design provides a significant change in diameter, which provides an effective means of using the fiber paths provided by over-braiding to create a mechanical locking effect. It also provides a higher surface area to promote adhesive bonding. The load vs displacement data is presented in Figure 49.

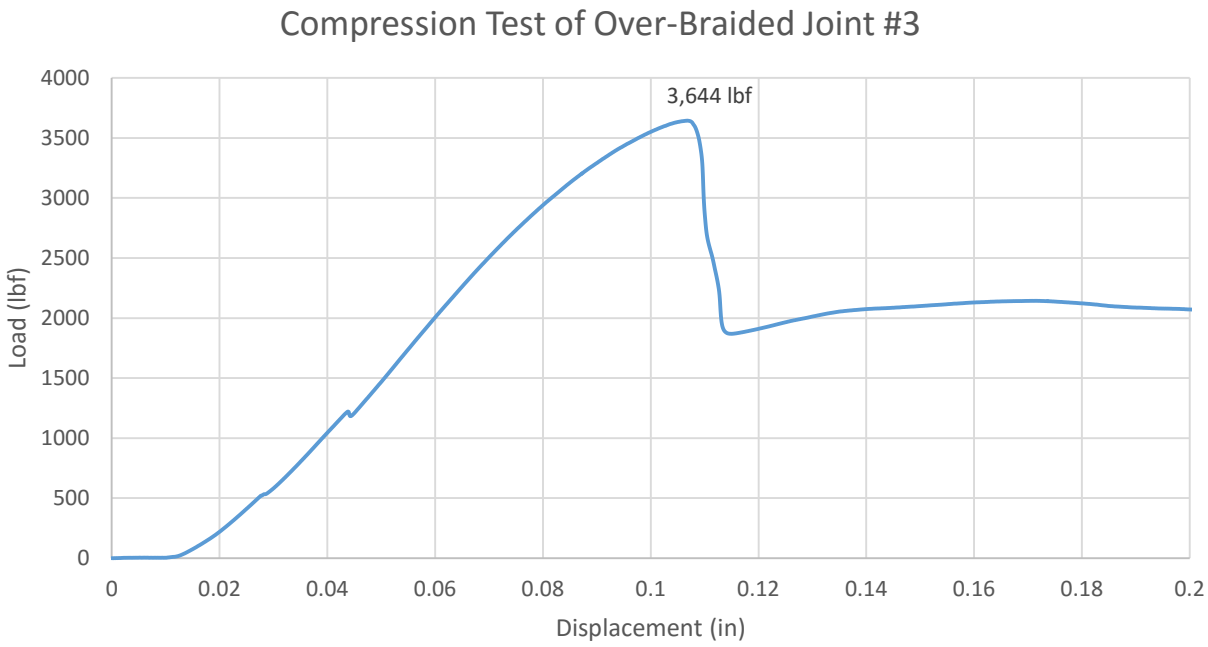

Figure 49 – Load vs Displacement Data for Over-Braided Joint #3

The primary mode of failure for joint #3 was a failure in the composite taper, although the insert showed minor dislodging, a displacement of 0.010 inches. This is registered in the above data as the slight peak around the 1,200 lbf mark. After this, the mechanical locking of the insert design allowed for load to continue to pass into the composite, until failure at 3,644 lbf. The failure was in the region of the taper at the end of the metal insert, shown in Figure 50.

Figure 50 – Failure of Over-Braided Joint #3

Over-braided joint #4 incorporated the most complex insert design that was evaluated, the quad taper with pins design, seen in Figure 25. This design featured two sets of tapers, as well as pins to inter-lock into the fibers. The load vs displacement data is displayed in Figure 51.

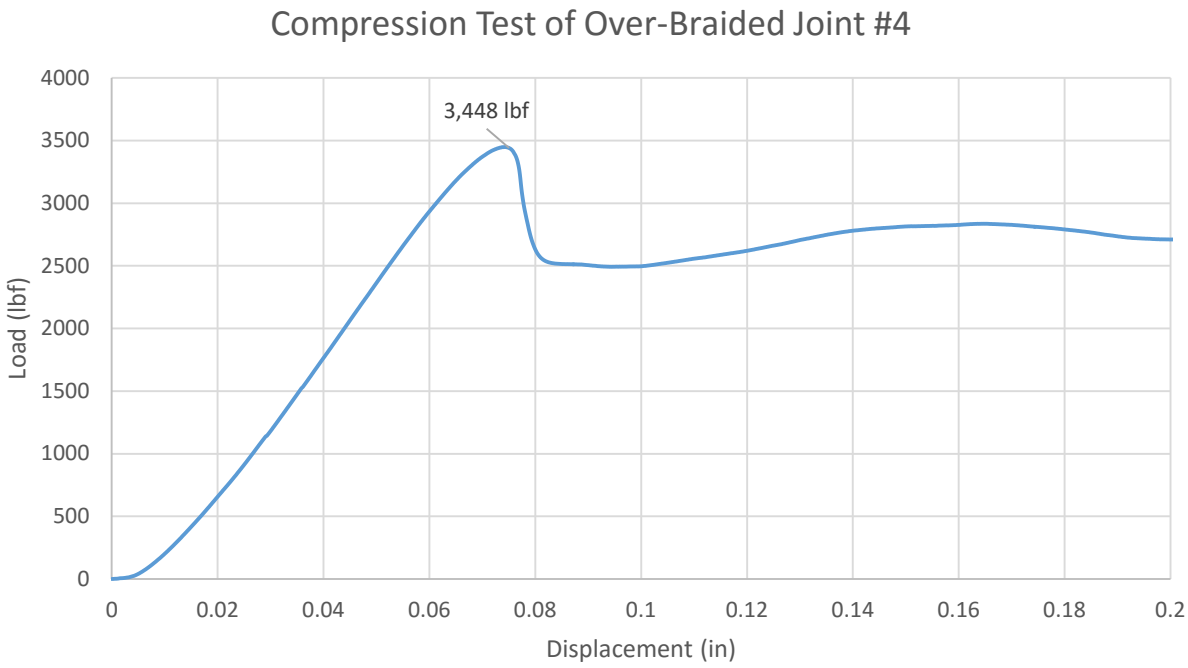

Figure 51 – Load vs Displacement for Over-Braided Joint #4

This data shows that there was no dislodging or debonding of the insert from the composite. The only failure of the joint occurred in the composite, at the same location as the over-braided joints #2 and #3. This failure occurred at a peak load of 3,448 lbf and is shown in Figure 52. Inspection of the insert post-test revealed that there was no discernable shifting of the insert within the composite.

Figure 52 – Failure of Over-Braided Joint #4

Section 3.6 – Discussion of Test Results of Taper Joints with Metallic Insert

The joints fabricated and evaluated in Chapter 3 represent three unique manufacturing methods and also evaluate various methods of integrating the metal insert. Filament winding, hand lay-up, and over-braiding were evaluated for means of manufacturing. Adhesive bonding and mechanical interlocking, and combinations thereof, were evaluated as approaches to incorporate a metal insert into the joint. Due to the inherent differences between these processes, the joints must be judged with the relevant process and its characteristics taken into consideration.

Section 3.6.1 – Summary of Filament Wound Joints Testing Results

The filament wound joints manufactured in Section 3.2 investigated two metal insert designs as well as two methods of integration. Filament wound joint #1 and #2

investigated the influence of insert design on the mechanical locking effect by comparing the V-groove and the double taper insert design. Filament wound joint #2 and #3 evaluated the effect of mechanical locking versus a significant adhesive bond.

Filament wound joint #1 was fabricated with a V-groove style insert and relied primarily on a mechanical locking effect. The insert was partially dislocated at a load of 1,985 lbf, although the joint continued to sustain load up until 2,500 lbf. Filament wound joint #2 was fabricated similarly to #1 but included a double taper-in style insert. This joint failed in the composite, without a discernable dislocation of the insert at 1,626 lbf. This data indicates an inequality between the FRP composite materials in each joint, despite similar lay-up schedule. This is most likely due to the manual control of tow placement and tension, which inherently leads to variation. As such, it is difficult to draw direct conclusions from this data. Joint #1 sustained 79.4% of its failure load prior to the dislodging of the insert. Joint #2 appears to have sustained 100% of its failure load without an insert failure, though additional testing is necessary to confirm. Filament wound joint #3 was manufactured in similar fashion to joint #2, but with the addition of a layer of film adhesive to provide an adhesive bond to supplement the mechanical locking of the insert. Joint #3 experienced an insert failure at 3,125 lbf, followed by failure within the composite structure at 3,405 lbf. Again, the disparity in the composite structure due to process variation prevents a direct comparison. Joint #3 sustained 91.8% of its failure load prior to insert failure. This indicates the inclusion of a film adhesive is an effective method to promote the transfer of load from the insert to the composite. Figure 54 shows a comparative plot of all 3 filament wound joints.

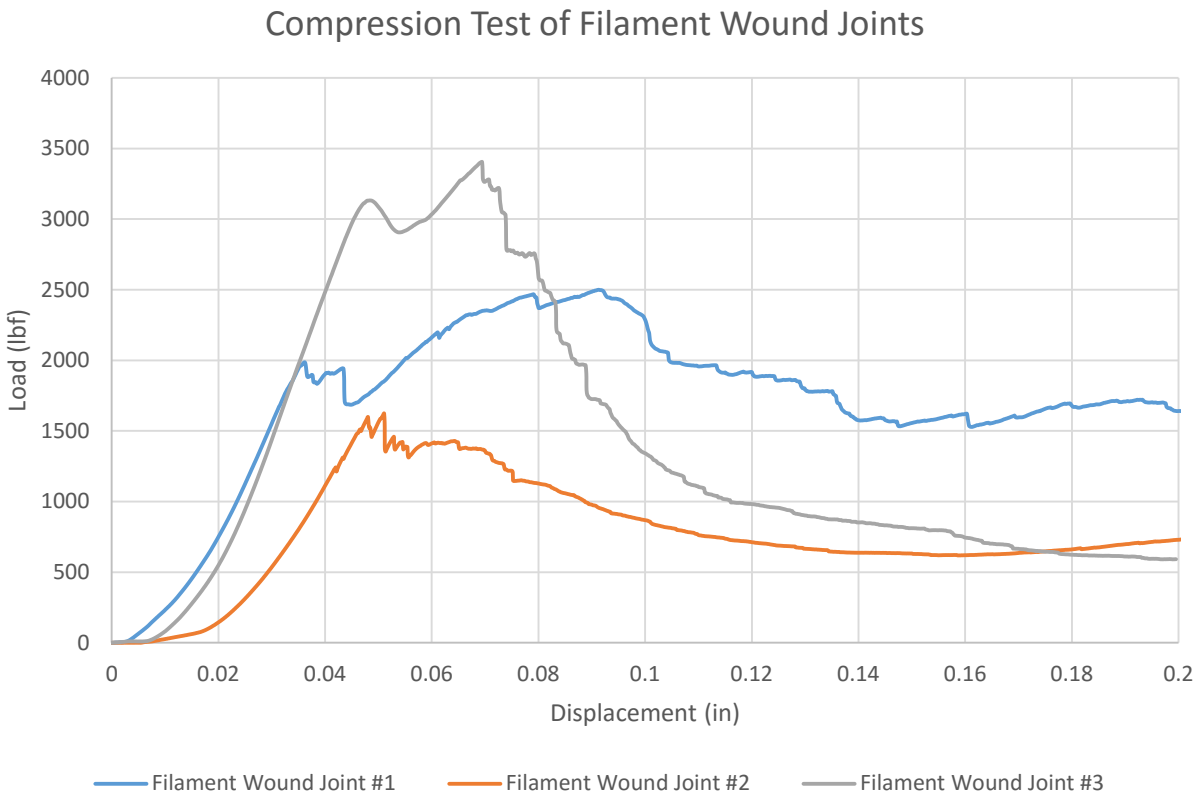

Figure 53 – Load vs. Displacement of Filament Wound Joints

Although the data gathered from these tests is difficult to discern due to process variation, several key points can be observed. Firstly, all filament wound joints failed in compression at a higher load than can be supported by the standard O-ACS test specimen, approximately 1,100 lbf. It is anticipated that these joints would sustain a much higher load in tension, as such behavior is common in carbon FRP materials. Additionally, the addition of an adhesive bond greatly increases the effectiveness

Section 3.6.2 – Summary of Hand Lay-up Joint Testing Results

The fabrication of a tapered composite joint with an integrated metal insert by hand lay-up focused on the evaluation of relying solely on an adhesive bond to integrate the insert. 3M DP 460 epoxy was used to bond a cylindrical metal insert into the cured composite joint. The adhesive manufacturer does not provide bond strength data for

bonds between Aluminum and FRP substrates, but a reasonable estimation can be gained from the provided FRP-FRP bond strength of 1,000 psi [17]. Given the diameter (0.75 in.) and height (1 in.) of the insert, surface area is calculated to be 2.356 in^2. An adhesive failure occurred in the joint at a load of 2,108 lbf, indicating a bond strength of 895 psi. This low bond strength may be improved by substituting an adhesive that is more suitable for dissimilar substrates.

Section 3.6.3 – Summary of Over-Braided Joints Testing Results

Four over-braided joints with integrated metallic inserts were tested in compression. The focus of the tests were to determine the strength of the composite and evaluate the effect of insert design on joint strength. All joints, except for joint #1, were manufactured with 3 layers of 64 end Hexcel 6k AS4C carbon fiber. As discussed in Section 3.5.3, joint #1 was over-braided with 2 layers of 32 end Hexcel 6k AS4C carbon fiber; one third of the fiber reinforcement of the other joints. Figure 54 shows a comparative plot of all over-braided joints.

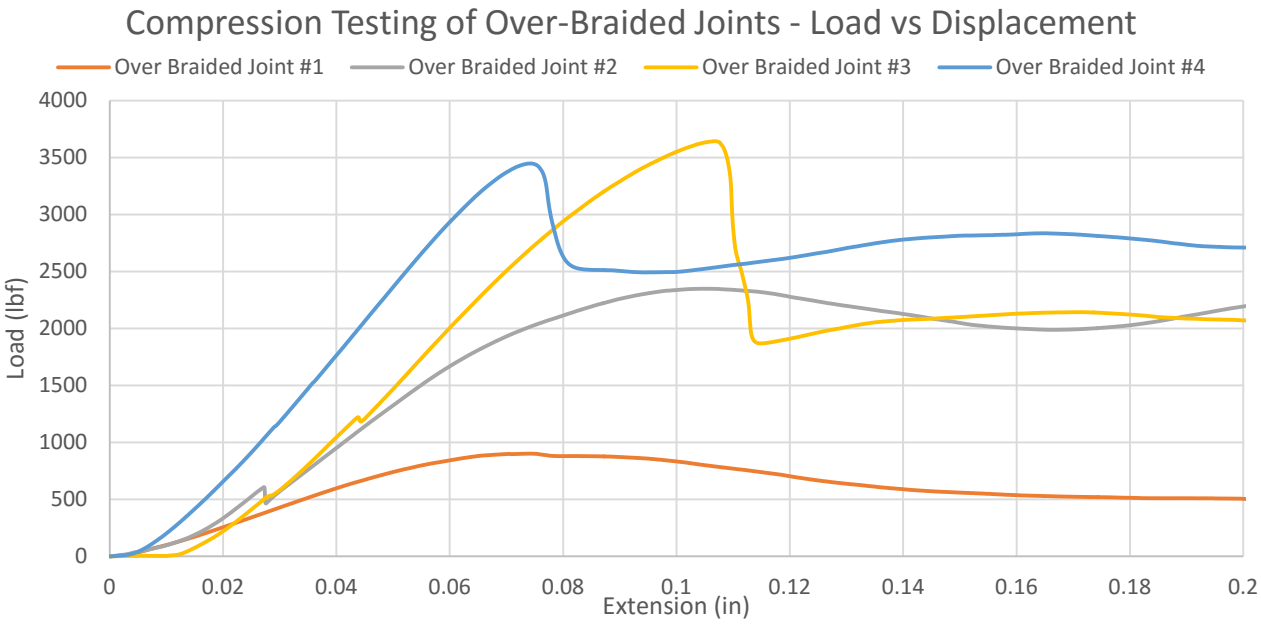

Figure 54 – Comparison of Over-Braided Joint Test Data

Thus, it was expected that joint #1 would fail at a significantly lower load than the remaining joints. Accordingly, joint #1 experienced failure in the composite at 902 lbf, with no noticeable insert failure. While this is a considerably lower failure load, it is consistent with the failure loads of the joints with increased amount of reinforcement. Considering joint #1 has a third of the reinforcement, tripling the failure load gives approximately 2,700 lbf. Considering the average failure load of joints #2 – #4 is 3,365 lbf, 2,700 lbf is in-line with this data. The approximately 500 lbf deficit may be attributed to the geometry of the diamond braid architecture. Because the fibers interlace with each other in a 1/1 pattern, there is a considerable increase in the amount of crimp in the fiber path compared to normal (2/2) braiding geometry. Fiber crimp decreases the percentage of the fiber that is in-line with the load and thus impedes effective load transfer.

Joint #2 uses a V-groove style insert, the same as filament wound joint #1. Over-braided joint #2 underwent an initial insert failure at 606 lbf, but continued to sustain load up to 2,963 lbf at which point the composite had failed. Because both filament wound joint #1 and over-braided joint #2 experienced an insert failure and contained the same insert, the importance of complimentary fiber paths and insert designs can be assessed. The V-groove style insert was dislodged at a load of 2,500 lbf when filament wound, yet it failed at a mere 606 lbf when integrated via over-braiding. The filament wound fiber paths nest densely into the recessed V-grooves because of the circumferential nature of the grooves and the fiber paths. Contrastingly, the helical fiber paths created via over-braiding do not effectively lay down into the circumferential V-grooves. Despite the initial dislocation of the insert, the over-braided joint was able to sustain a higher load than the filament wound joint, an indication that the over-braided composite is of higher

strength than the filament wound composite joint in this case. As the ineffectiveness of the V-groove style insert was anticipated for over-braided joints, the following joints feature insert designs more complimentary to braided fiber paths.

Joint #3 uses a double taper-out design insert, which was designed to vary the cross section in a manner that complimented the over-braiding process. The joint experienced a slight displacement of 0.010 inches and reached a load of 3,644 lbf prior to composite failure. This test shows that an effective insert design can provide a meaningful mechanical locking effect between the composite joint and the insert. The Double taper-out design uses a change in cross-section diameter to lock it into the over-braid. The benefit of the over-braiding process is the ability of the fibers to braid tightly around the mandrel, minimizing the need for a secondary operation to provide fiber compaction, such as vacuum bagging. This constriction of the fibers around the insert provided enough mechanical locking to withstand the force until failure of the composite.

Joint #4 was produced with an evolution of the double taper-out design, the quad-taper with pins. This insert design features 4 changes in cross-section diameter to allow the fibers to constrict and trap the insert. In addition to the changes in diameter, the insert featured 8 pins that were press-fit into the circumference of the first and last taper. As the fibers braided around the insert the pins were interlocked between the fiber crossover points. The joint experienced failure of the composite laminate at 3,448 lbf and the insert remained entirely fixed within the composite. Despite joint #3 reaching a higher load, joint #4 is noteworthy due to the unfaltering insert/composite interface.

Section 3.7 – Conclusions from Evaluation of Taper Joints with Metallic Insert

The primary feature of this joint design was the integration of the metal insert with threads; allowing for a multitude of possible connection types. The methods of manufacture investigated in this chapter are in effort to determine the best possible way to integrate such an insert. Filament winding, hand lay-up, and over-braiding all have their unique benefits and drawbacks. The most appropriate method will be determined based upon each situation's unique design requirements.

Filament winding presents a process that is easily automated and relatively low cost for a high output. By utilizing pre-impregnated fiber tows a precisely controlled resin content is possible, resulting in a very lightweight and optimized joint. However, a CNC filament winder would be necessary to accurately and repeatedly control fiber paths and tension. Should filament winding be chosen as the manufacturing method, a V-groove style insert or a design with similar features would provide a high degree of mechanical locking. Additionally, the inclusion of an adhesive film between the insert and composite laminate was shown to be very effective. Although the joints manufactured for testing did not feature an annular channel to increase bonding area, this feature would be straightforward to incorporate into the manufacturing process.

Hand lay-up of a tapered joint with a metallic insert would provide the most simple and low cost method of production. Lay-up would utilize braided carbon sleeve of the appropriate diameter and a suitable resin system. Resin content would be difficult to control and may lead to a joint with unnecessary mass. Additionally, a reliable method of providing fiber compaction during cure would be necessary. Due to the shape of the joint, a conventional vacuum bagging method is unlikely to provide satisfactory surface finish. A mold or trapped rubber mold may be

viable alternatives. This process also has the additional step of secondary bonding the insert into the composite. While it has been shown that this may provide adequate strength, it does add an additional point of failure within the joint. Proper surface preparation for the composite and the insert is critical for this method of incorporating the insert.

Over-braiding is the most sophisticated and intricate of the processes evaluated. It is expected to be the most costly and time-consuming of the processes. Nevertheless, it would also produce joints of the highest quality. The tightly braided fibers provide a highly effective mechanical locking effect upon the insert; as well as aiding in fiber compaction. With a CNC braiding machine like the one used, it would be possible to fully automate the over-braiding process and accurately control braid angle to optimize the composite properties. The method of resin impregnation is one that would need to be evaluated in more depth. An ideal method would be a resin infusion process, although this would require a costly mold. Application of resin by hand is feasible, provided the resin is able to fully penetrate the tightly braided layers of fiber and a mold ensure proper compaction and surface finish. An insert with changes in cross-section diameter or shape is necessary for effective mechanical locking. Press-fit pins, while adding complexity to insert manufacture, have been shown to more effectively prevent insert failure.

As for insert design, it is critical to pair an insert design with a complimentary manufacturing process. In the case of filament winding it is necessary to include circumferential features that trap the circumferential fiber paths. Inserts that feature substantial, yet gradual, changes in cross-section are effectively trapped in the tight braid. Insert weight should also be taken into consideration, as an excess of fiber trapping features that far supersede the load requirements of the joint add unnecessary weight. Additionally, insert material is an important choice. Aluminum was chosen in these joints due to low cost and ease of manufacture. However,

if aluminum were to be used for a production joint, steps to prevent galvanic corrosion would need to be taken. A metal such as titanium would provide weight savings without compromising strength.

In summary, three viable methods of producing a composite taper joint with an integrated metal insert were proposed. Prototype joints were fabricated for testing of joint strength and to provide comparisons between insert designs and integration methods. While some designs showed evidence of insert failure in the form of becoming dislodged, all designs that utilized a mechanical locking effect were able to continue to sustain increasing load to the point of composite failure. Insert designs were shown to be more effective at providing mechanical locking when paired with manufacturing process that provided a complimentary fiber path. These joints sustain peak loads of approximately 2,000 lbf to 3,500 lbf in compression. When used with a standard O-ACS, this results in a safety factor of greater than 2, as the standard O-ACS test specimen considered in this research fails under approximately 1,100 lbf. An additional benefit of this tapered composite design is the failure mode. Unlike most composite structures that undergo brittle failures, the taper of the joint acted similar to a crash cone structure utilized in some automobiles; that is to say the failure was gradual and controlled. These joints are expected to reach much higher loads when loaded in tension, as is the nature of composite structures in compression along the length. In conclusion, a tapered composite joint with an annular channel provides a lightweight, strong and versatile method of joining O-ACS.

Chapter 4 – Permanently Bonded Joints

Certain design criteria may call for a permanent means of affixing O-ACS to one another to create a permanent assembly. As such, a method of rigidly affixing O-ACS components to each other was developed. This chapter details two joining concepts that join O-ACS via secondary bonding. The initial concept was a simple splice joint; consisting of a cylindrical component that matched the inner diameter of the O-ACS that were to be joined. While this design provided a lightweight and simple joint, a design yielding higher sustained loads was desired. As it has been previously stated, the inherent lack of surface area of O-ACS presents a challenge when adhesive bonding is the primary fixturing method. As such, the simple splice joint can be improved by increasing bonding area. An evolution of the splice joint resulted in a coupling that doubled the bonding area of the splice joint.

Section 4.1 – Composite Splice Joint

A splice joint is a common method of joining two cylindrical structures. It consists of a cylindrical component that has an inner diameter or outer diameter that matches the complementary diameter of the structures to be joined. An internal splice joint, wherein the splice component has an outer diameter that closely matches the inner diameter of the O-ACS, was chosen due to the uncontrolled nature of the outer diameter dimension of O-ACS.

Composite splices were manufactured via the following methods. A mandrel was turned on a lathe to the desired diameter, the diameter being chosen based upon the ply layup and desired final outer diameter of the splice. A layup schedule consisting of 2 plys of 1.75 in. diameter braided carbon sleeves was chosen to supply desired strength and stiffness. As each braided sleeve had a thickness of approximately 0.06 in., the aluminum mandrel was turned to an

outer diameter of 1.63 inches. A release agent, Frekote 770-NC, was applied to the mandrel and epoxy was applied to the two sleeves and cured on the mandrel. Heat shrink tubing was applied to ensure proper lamination and provide and an even outer surface. The cured splice was cut to the desired length, surface prepped for bonding, and bonded into the O-ACS to be joined. Table 4 details materials used to manufacture the splice joints.

Table 4 – Materials Used for Splice Joint

Material	Description
Carbon Sleeve	Highland Composites 1.75” Sleeve
Matrix	Araldite LY 8601 Epoxy Resin
Surface Preparation	Media Blasted with Aluminum Oxide
Bonding Adhesive	3M DP 460 Epoxy Adhesive

Three lengths of splice were chosen for testing: 1.0, 2.0, and 3.0 inches. Additional 1.0 and 2.0 inch splices were manufactured for an evaluation of the effect of surface preparation on joint strength. O-ACS were potted in pipe nipples for fixturing in an Instron testing machine to undergo tensile testing. Figure 55 shows the varying lengths of splices; with the splices on the right having been surface prepped by media blasting. Figure 56 shows a detailed view of the difference in surface roughness before and after media blasting.

Figure 55 – 1”, 2”, and 3” Splices

Figure 56 – Un-prepped Composite vs. Media Blasted

Section 4.2 – Composite Coupler Joint

The desire to increase the bondable surface area in the splice joint without increasing the splice length resulted in the following coupler design. By integrating an annular channel into the composite, a coupler joint was created. The channel is designed to encapsulate the end region of the O-ACS and filled with bonding adhesive. This design effectively doubles the surface area of the splice joint for a given bond length. By fully enclosing the adhesive, a more refined aesthetic is also achieved.

A silicone rubber tool was created to form an annular channel during layup and cure. In order to achieve the exact dimensions required a 3D printed part was produced using a FDM machine. This printed part was then cast in silicone rubber to create a mold. This mold was then sealed, released, and used to create subsequent silicone tooling in the shape of the original 3D printed part (Figure 57). This silicone tooling was inserted in-between plys during the layup and removed after curing; shown in Figure 58. O-ACS were then bonded into the annular channel and potted in pipe nipples for testing; seen in Figure 59 and Figure 60. Table 5 details the materials used for the manufacture of this joint.

Figure 57 – 3D Printed Master and Silicone Tooling

Figure 58 – Coupler Joint Lay-up Process

Figure 59 – Cured Coupler Joint

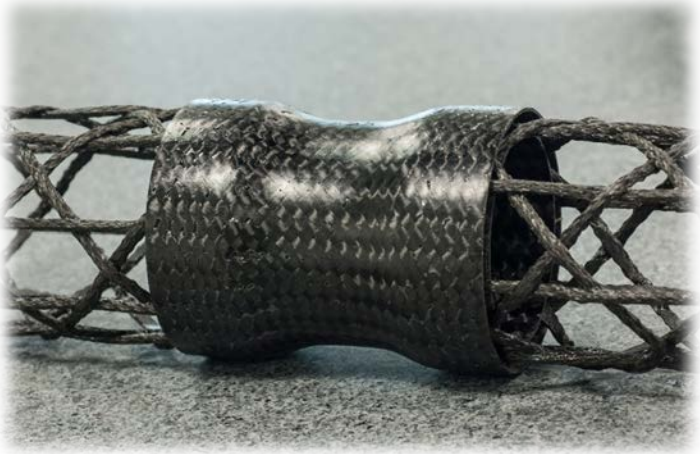

Figure 60 – Coupler Joint with Bonded Open-Structures

Table 5 – Materials for Coupler Joint

Material	Description
3D Printed Master	Hyrel System 30, N-Vent Filament
Silicone Rubber	Smooth-On EZ-Brush platinum silicone
Fiber Reinforcement	Highland Composites 1.75” Braided Carbon Fiber Sleeve
Matrix	Araldite LY 8601 Epoxy Resin
Bonding Adhesive	3M DP 460 NS Epoxy Adhesive

Section 4.3 – Evaluation of Permanently Bonded Joints

The geometry of these 180° joints was chosen to simplify the manufacture and test phase of this case study. However, based upon the data gathered from the testing, it would be a logical progression to create a family of splice and coupling joints that include elbows, three-way, and

four-way joints. Data from the testing of splice and coupler joints is presented in the following sections.

Fixturing of these joints for testing was achieved by potting the joined O-ACS into threaded pipe nipples with epoxy resin. These pipe nipples were threaded into pipes that could be fixtured into the Instron testing machine. Particular care was taken to ensure concentricity between the O-ACS and the pipes they were potted in. An alignment jig (Figure 61) was fabricated with U-channels and pipe couplers to ensure ideal alignment. All pipe nipples were media blasted to promote bonding. Once potted, the specimens could be threaded into pipe reducers and in turn into pipes that could be pinned into the Instron. This configuration is shown in Figure 62.

Figure 61 – Potting Alignment Jig

Figure 62 – Fixturing of Potted O-ACS

The tension testing of these samples was carried out in the closest accordance possible to ASTM D3039. Due to the inability to monitor strain during testing, a constant cross-

head travel of 2mm/min was used. Cross-head travel and load was recorded. The method defined above was used for the evaluation of all splice and coupler joints, the resulting data of which is presented in the below sections.

Section 4.3.1 – Testing of Composite Splice Joints

The five samples that were joined via a composite splice joint were potted into pipe nipples with epoxy as described in the above method. The five samples consisted of three lengths: 1.0, 2.0, and 3.0 inches. Additional samples were prepared for 1.0 and 2.0 inch lengths for an evaluation of the importance of surface preparation. These potted samples ready for testing are seen in Figure 63.

Figure 63 – Potted Splice Joints

The load vs displacement data for each of the five samples has been compiled into the following graph.

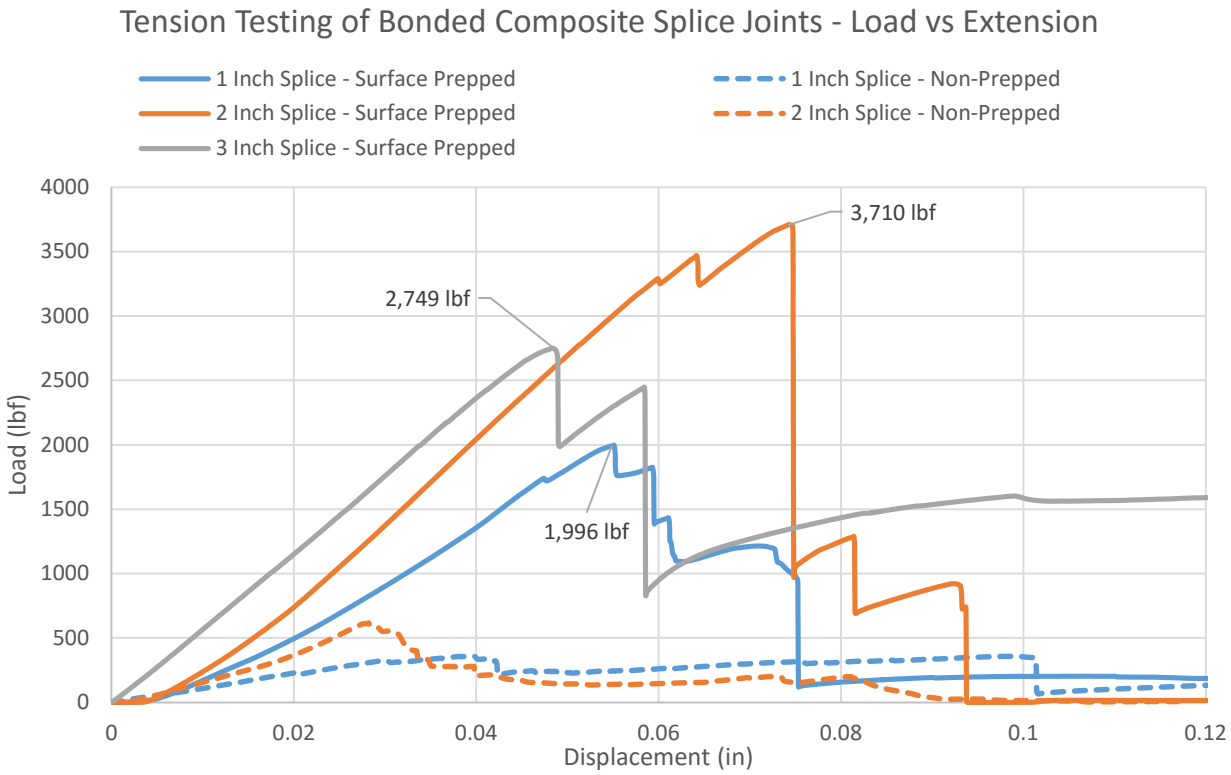

Figure 64 – Load vs Displacement Data for Composite Splice Joints

As shown by the above data of Figure 64, the un-surface prepped samples exhibited a significant reduction in bond strength. Adhesive debonding of the 3M DP460 and the composite splice was seen in all 1.0 and 2.0 inch samples. The 3.0 inch sample showed some signs of onset of debonding, but the potting failed prior to realization of ultimate load. An example of a typical adhesive debonding failure of a splice joint is shown in Figure 65.

Figure 65 – Failure of 1 inch Splice Joint

Section 4.3.2 – Testing of Composite Coupler Joint

A composite coupler joint was fabricated as discussed in Section 4.2. The annular channels were filled with 3M DP460 structural epoxy and O-ACS were inserted for bonding. Concentricity of the joined O-ACS was ensured by fixturing in a lathe and use of a drop dial indicator. These, now joined, O-ACS were potted into pipe nipples as described in Section 4.3. The joined O-ACS potted into pipe nipples is seen in Figure 66.

Figure 66 – Coupler Joint Potted for Testing

The data from the tension test of the coupler joint is presented in Figure 67. The joint showed no failure in the coupler or bond region. Failure initiated in the O-ACS axial cord-pregs at a load of 5,577 lbf. This failure is shown Figure 68 and Figure 69.

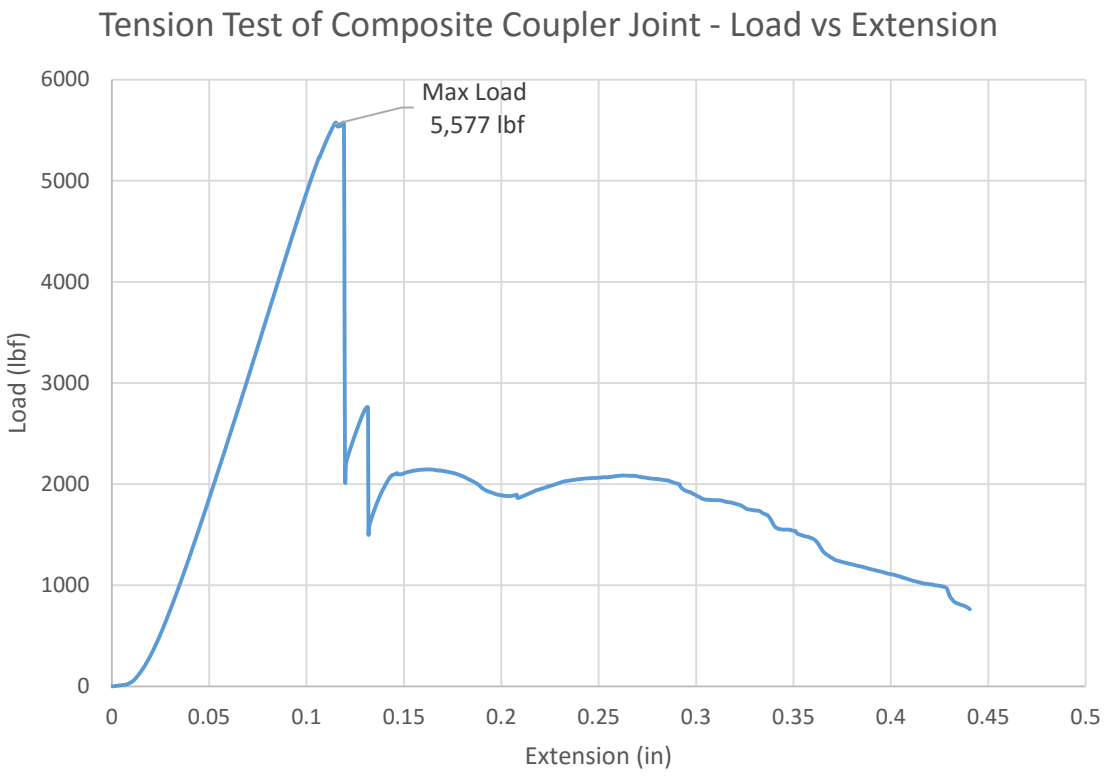

Figure 67 – Load vs Displacement for the Composite Couper Joint

Figure 68 – Coupler Joint Post-Failure

Figure 69 – Detail of Joined O-ACS Failure

Section 4.4 – Discussion of Test Results of Permanently Bonded Joints

Permanently bonded joints can provide a strong and reliable method of connecting O-ACS when disassembly is not a requirement. Given proper surface preparation and a suitable adhesive a predictable and simple connection may be created. The testing of several lengths of splice confirmed a linear relationship between splice length and bond strength. It also highlighted the importance of proper surface preparation. The coupler joint demonstrated the benefits of significantly increasing bond area without adding additional material.

Section 4.4.1 – Summary of Splice Joint Testing Results

The testing of 3 lengths of splices revealed the linear relationship between splice length and bond strength, as expected. The evaluation of surface preparation also

reinforced the importance of surface preparation. The strength of the adhesive bond was calculated by determining the total length of the bonded cord-pregs (Equation 2).

$$Total\ Length\ of\ Bond\ Area = (0.5 * L * A) + \left(H * \left(\frac{0.5 * L}{\cos(\theta)}\right)\right)$$

$$L = Length\ of\ Splice$$
$$A = \#\ of\ Axials$$
$$H = \#\ of\ Helicals$$
$$\theta = Braid\ Angle$$

Equation 2

Using this 'total length of bond area' an approximation of surface area was calculated using Equation 3. This equation uses the formula for the surface area of a cylinder, truncating the cylinder ends, and halves it due to the bond area only being on the inner diameter of the O-ACS.

$$Bond\ Area = \frac{1}{2} * (2 * \pi * r * Total\ Length\ of\ Bond\ Area)$$

Equation 3

Table 6 shows the calculated bond strength for each splice tested. The technical data sheet provided by the adhesive manufacturer specifies a bond strength of 1,000 psi for FRP bonded to FRP in an overlap shear test [17]. The resulting bond strength for a properly surface prepped splice is in excess of 1,000 psi. This data suggests a fivefold decrease in strength if proper surface preparation is neglected.

Table 6 – Bond Strength of Splice Joints

Splice Length (in)	Surface Prep	Total Bond Length (in)	Bond Area (in^2)	Peak Load (lbf)	Bond Strength (psi)
1	Media Blasted	11.61	1.82	1996	1094.07
1	None	11.61	1.82	357	195.68
2	Media Blasted	23.23	3.65	3710	1016.78
2	None	23.23	3.65	615	168.55
3	Media Blasted	34.84	5.47	2748	502.09

$\theta = 45°$

r = 0.05 in.

In the case of the 3 inch splice, it was observed that the potting failed prior to the failure of the adhesive bond. However, using the average bond strength derived from the

surface prepped 1.0 and 2.0 inch splice, an approximation of a failure load can be calculated. If the potting for the 3.0 inch splice had not failed, it is reasonable to expect a maximum sustained load of approximately 5.776.5 lbf. The linear relationship between splice length and maximum load for surface prepped specimens is seen in Figure 70.

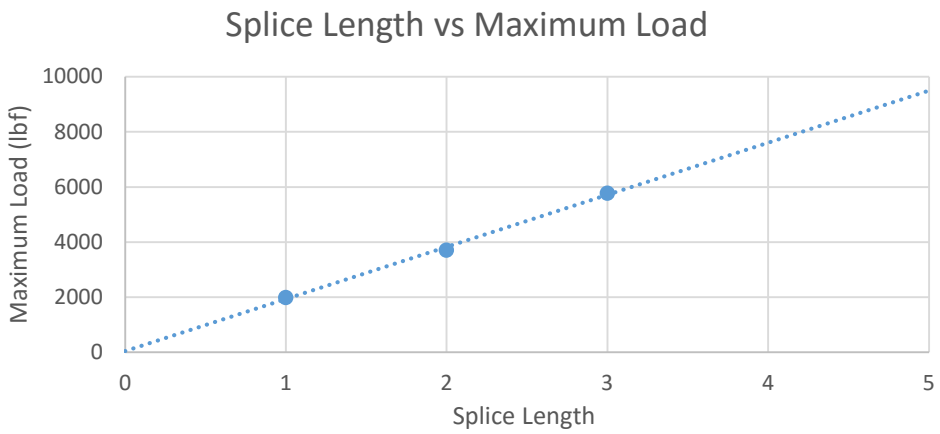

Figure 70 – Splice Length vs Max Load

This data has shown that a splice joint is a reliable and predictable method of connecting O-ACS. By utilizing manufacturer provided strength data, an accurate estimation of bond strength can be achieved through use of the above equations. Additionally, given the maximum sustained loading of the O-ACS, an optimum splice length of bond length can be calculated.

Section 4.4.2 – Summary of Coupler Joint Testing Results

The primary purpose of the coupler joint was to increase bond surface area without increasing weight. Its secondary purpose, purely aesthetic, was to conceal the adhesive. The coupler joint was manufactured with two braided sleeves of carbon fiber; equivalent to the lay-up of the splice joints. The annular channel for this coupler was 1 inch deep on each end, allowing for comparisons to the 2 inch splice to be made. Therefore, nearly identical weight per unit length can be achieved for these two types of

joints. The weight of per unit length of the coupler joint is 0.0207 lb/in, compared to 0.0170 lb/in for the splice joints. By integrating the annular channel, the surface area of the O-ACS doubles due to the ability to utilize the outer surface of the O-ACS as a bond surface. Therefore when calculating bond area, the 0.5 multiplier is removed from Equation 3, resulting in Equation 4. The total bond length formula remains unchanged (Equation 2).

$$Bond\ Area = 2 * r * Total\ Bond\ Length$$

Equation 4

Utilizing these equations, a total bond area for the coupler joint is calculated to be 7.3 in^2; double that of a splice with equivalent length. Due to this significant increase in bond area, the joint and adhesive bond was able to surpass the failure load of the O-ACS. The O-ACS failed at a load of 5,577 lbf. Assuming the same adhesive bond strength of 1,000 psi, it is calculated that the coupler joint would not see an adhesive failure until approximately 7,300 lbf with a 1 inch deep annular channel. A splice joint that sustains an equivalent load would measure 3.8 inches and weigh 0.0627 lbs.; nearly a 50% increase in weight.

Section 4.5 – Conclusions from Evaluation of Permanently Bonded Joints

Permanently affixing O-ACS to each other by means of adhesive bonding is a simple and reliable method of creating O-ACS assemblies if proper bonding techniques are adhered to. While this method may not be feasible for some design requirements, due to its permanent nature, there are many scenarios where such a means of fixturing is acceptable. The data in Section 4.4 shows that an adhesively bonded joint can be reliably designed once the adhesive bond strength is characterized for the O-ACS and complimentary substrate. Adhesive bonding

allows for a lightweight joint while providing a reasonably high strength joint. Additionally, it was shown that methods of increasing the bond area of the O-ACS has a significant effect on strength and weight savings. As a result of this investigation, it is recommended to incorporate a method of encapsulating the region of the O-ACS to be bonded, as the annular channel of the coupler joint does. This minimizes the length of the bonding region while maximizing bond surface area. As a result, weight savings can approach 50% compared to a bond only utilizing the inner surface of the O-ACS. Additionally, this method encloses the adhesive, which may provide aesthetics critical to commercialization.

Chapter 5 – Compressed Bi-Axial Spring Joints

One set of design criteria defined a joint that could be assembled with minimal resources and in a short amount of time. This type joint must be readily field deployable with limited resources, tools, and time. As such, a trade-off in maximum strength for these characteristics is considered allowable. This concept calls for a joint that allows for O-ACS members to be cut to length and without any further preparation be assembled into a rapidly usable structure. The joint must also be able to be quickly dismantled, as well as being reusable. Previously presented concepts have met some of these design criteria, though all involve timely bonding procedures or O-ACS members that have been specially prepared or manufactured.

Section 5.1 – Bi-Axial O-ACS

This concept involves the use of a particular subset of O-ACS that possess the unique characteristic of flexibility. O-ACS of conventional architecture are a tri-axial braided structure. However, by removing the axial yarns, a bi-axial O-ACS may be produced. These structures can possess a unique range of characteristics, vastly different from a traditional O-ACS; a range of flexibility, high Poisson ratio, and spring-like behavior. Currently, there is limited research into these unique structures and their properties. Based on hands-on observations, a concept utilizing the high Poisson ratio and spring-like characteristics of these structures was developed. By subjecting a bi-axial O-ACS to a relatively trivial compressive longitudinal force, the structure will react by shortening longitudinally while substantially increasing in diameter. This is the primary mechanism upon which this joining concept functions.

Section 5.2 – Compressed Bi-Axial Joint Concept and Fabrication

A joint concept was developed that utilizes the previously described mechanism as a means to create a large amount of friction between two nested O-ACS. By nesting a bi-axial O-ACS inside of two conventional O-ACS members and applying a compressive force to the bi-axial structure, the bi-axial structure responds by expanding outward against the rigid O-ACS members and locking them in place. By employing a simple mechanism to compress the spring, the joint can be readily assembled and disassembled.

The initial proof-of-concept joint was designed be a 180° splice type joint that relied on the surface friction generated by the expanding bi-axial joint. Compressive force was provided via aluminum compression caps on a threaded rod. A partial cutaway view of the concept is seen in Figure 71; wherein the orange O-ACS members are to be locked together through the compression of the blue bi-axial spring via the aluminum compression caps on the threaded rod.

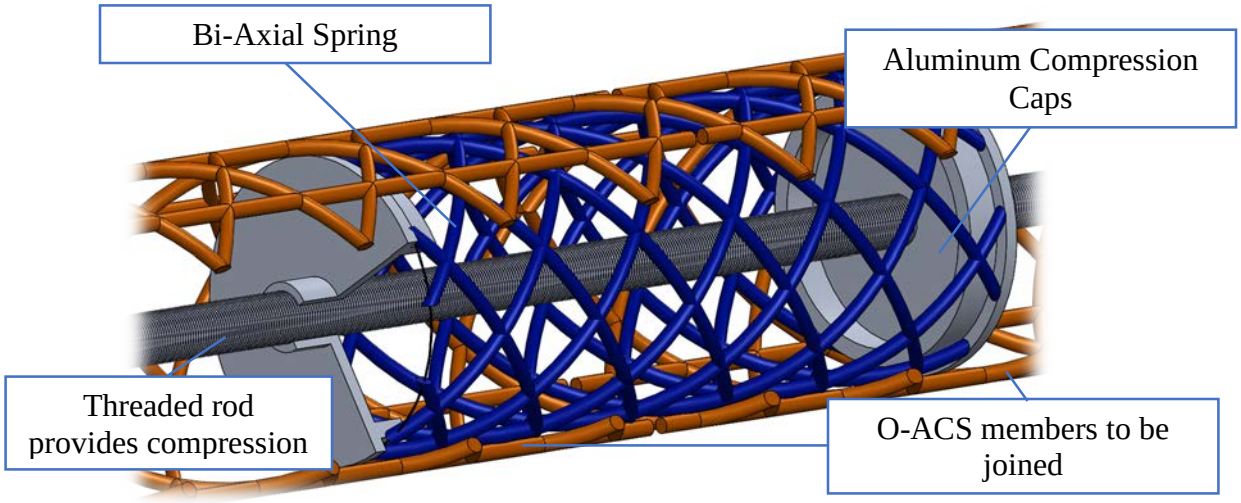

Figure 71 – Model of 180° Spring Compression Joint

The 180° splice joint was chosen to simplify fabrication and proof of concept testing. Firstly, a bi-axial O-ACS of suitable geometry and dimensions was manufactured. Due to relative limited research of bi-axial O-ACS, the following geometry was chosen based on hands-

on observations of previously manufactured structures. Table 7 details of the architecture of the bi-axial spring. A total of 12 braiders with cord-preg #22 (See Appendix for characteristics) was chosen to provide a high surface area to increase friction while still providing a limited compressive modulus. Mandrel diameter was chosen to produce a structure with an outer diameter of slightly less than 1.75 inches, such that it nested inside of the standard O-ACS. A 45° braid angle was chosen to provide a balance of compressive modulus and Poisson's ratio for the structure. A section of the bi-axial spring is shown in Figure 72.

Table 7 – Bi-Axial Spring Structure

Cord-Preg	#22
Mandrel Diameter	1.5 in.
Structure Outer Diameter	1.72 in.
# of Braiders	6 x 6
# of Axials	0
Braid Angle	45°

Figure 72 – Bi-axial Spring

Metallic compression caps were machined out of aluminum to fit inside of the bi-axial spring and threads cut to match the threaded rod. Figure 73 shows the bi-axial O-ACS fitted with the compression caps and prior to installation on the threaded rod. This assembly would be

nested inside of two standard O-ACS and the rod would be rotated to bring the caps together a set distance, thus compressing and expanding the spring inside the now locked O-ACS components.

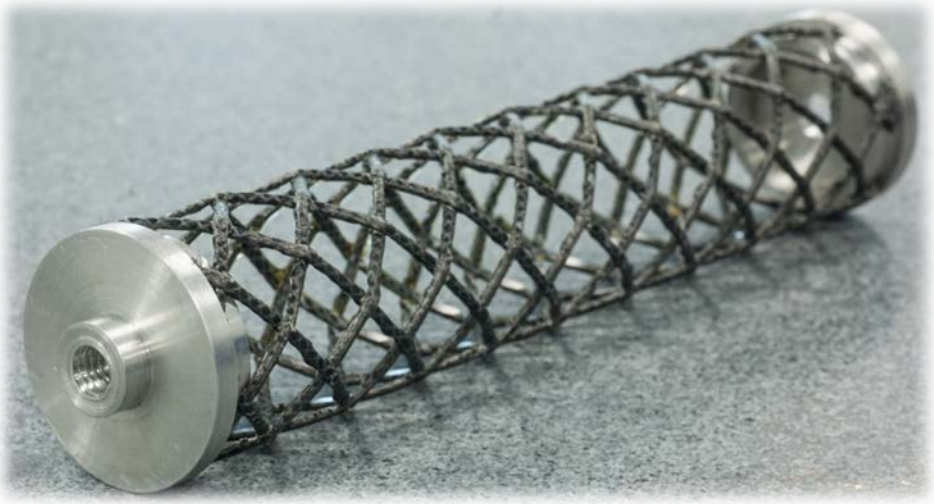

Figure 73 – Bi-axial Spring with Compression Caps Installed

Section 5.3 – Testing of Joint Strength based on Spring Length

There are many factors that influence the strength of this joint: length of spring, amount of spring compression and/or expansion, spring geometry, cord-preg, and surface preparation. Due to minimal research on bi-axial Open-Structures, the geometry and its effect on the compression/expansion of the spring were not investigated at this time. Because the locking mechanism relies mainly on friction, it was assumed that the most influential factor on this type of joint would be the overall length of the spring. As such, a set of tensile tests was carried out on O-ACS members spliced together with a compressed bi-axial O-ACS. All bi-axially O-ACS were manufactured as detailed in Table 7 and were used to splice together two standard O-ACS members that were potted in pipe nipples for fixturing. The joint strength was evaluated using springs of lengths 2.0, 4.0, 6.0, and 8.0 inches. (Figure 74).

Figure 74 – Varying Lengths of Bi-axial Springs Used for Testing

Each length of spring was installed in the compression assembly and inserted into the two potted O-ACS such that the midpoint of the spring was located at the point where the O-ACS members butted together. The spring was then compressed approximately 0.625 inches to adequately expand the spring and lock in the O-ACS. Spring compression of greater than 0.625 inches resulted in over compression of the spring and led to onset of failure in the bi-axial structure. Figure 75 shows how the test specimens were fixture into the Instron testing machine. The orange boxes highlight the O-ACS members being joined and the blue box highlights the internal bi-axial spring. The dashed line demarks the butt-joint of the two O-ACS to be joined.

Figure 75 – Specimen Fixtured for Tensile Testing

The tensile testing was conducted at a rate of 2 mm/min cross-head displacement. Results of tensile testing on spring lengths 4.0, 6.0, and 8.0 inches are shown in Figure 76. An attempt to test a 2 in. spring was made, but the spring failed prior to an effective amount of expansion. The maximum sustained load of each spring length is summarized in Table 8.

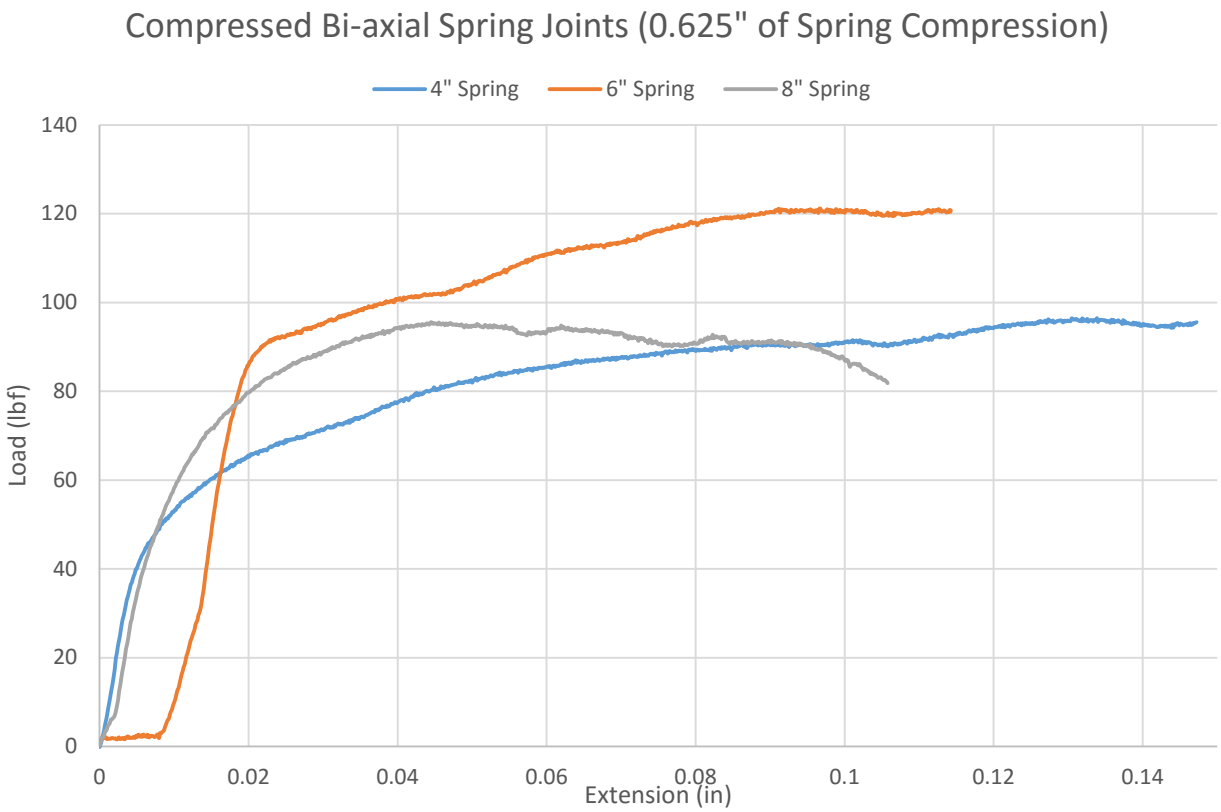

Figure 76 – Tensile Test of Compressed Spring Joint Data

Table 8 – Summary of Tensile Testing

Spring Length (in.)	Maximum Load (lbf)
4	96.5
6	121.2
8	95.6

As seen in Table 8, the maximum load sustained by the compressed bi-axial spring joint at 0.625 inches of spring compression was 121.2 lbf achieved with a spring length of 6.0 inches. Joint strength of the 4.0 and 8.0 inch springs were approximately equal. A thorough review of the resulting data follows in Section 5.4.

Section 5.4 – Discussion of Test Results of Compressed Bi-Axial Spring Joint

The compressed bi-axial spring joint was designed to provide a method of quickly and easily connecting and disconnecting O-ACS members with no prior preparation, save for

trimming to appropriate length. With this in mind, a decrease in joint strength is an acceptable trade-off. It is envisioned that these temporary structures would not be heavy load bearing structures and used primarily in light-duty and temporary space-frame type assemblies.

This data could be indicative of several scenarios. Initial conclusions would be that the optimal length of the evaluated lengths is achieved at 6 inches. This could be suggestive of a certain non-linear spring coefficient as length varies of this unique spring-like structure. This phenomenon has been postulated and research is on-going. Another possible scenario that could have resulted in this data is non-uniform compression of each length of spring, as exact measurements were not possible due to nested nature of the structures. However, it is unlikely that the minute differences in spring compression resulted in this data.

This joint was tested in tension because this was expected to be mode that would yield the lowest failure load. In compression, it is likely that the joint would have failed when the O-ACS structure reached its failure load of 1,100 psi or slightly below. This is assumed due to the likelihood that the end regions would have simply bared into each other until compressive failure, with the joint playing a minimal role other than maintaining alignment. It is suggested that this failure load may be below the nominal compressive load of an O-ACS owing to the unconstrained end regions of the cord-pregs.

Section 5.5 – Compressed Bi-Axial Spring 4-way Joint Prototype

Due to the appeal of a rapidly erectable joint for use with unmodified O-ACS, a prototype 4-way joint was designed and fabricated. The envisioned joint would be able to rapidly connect up to 4 O-ACS with only basic tools and allow for swift disassembly and reuse. Additionally, the O-ACS would not require modification prior to joining, save for cutting to the desired length. The primary use of such a joint would be in a space frame structure where loads are primarily

tension/compression forces. It was essential that the spring compression mechanism added minimal mass and was simple to operate. Figure 77 depicts a solid model of the prototype joint.

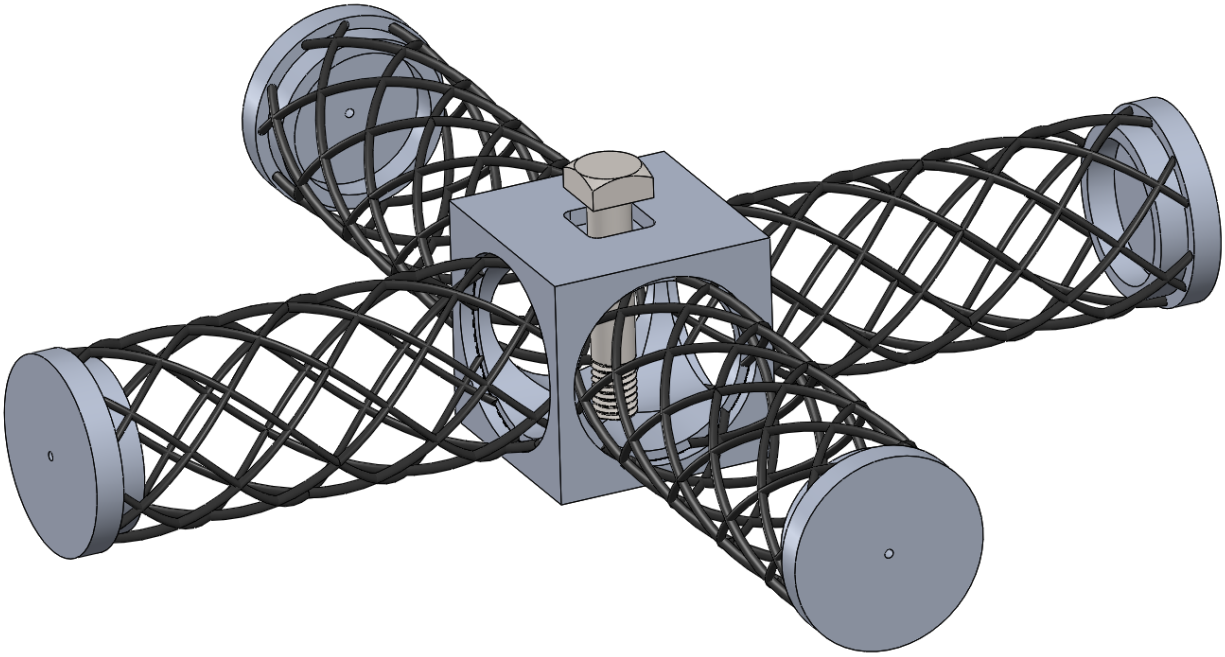

Figure 77 – 4-Way Compressed Spring Joint Model

An aluminum cube forms the central structure of the joint, to which 4 bi-axial springs are bonded. The central cube is bored out to reduce mass and provide a bonding surface for the springs. A centrally located bolt with thru-holes for a braided rope form the compression mechanism. The bolt acts as a winch for a braided rope that connects the end compression caps of the springs to the bolt. The square head bolt can be rotated to compress the springs and then locked in place by depressing it into the square recess in the cube to prevent and further rotation.

A billet of 6061 aluminum was milled into a 2 x 2 inch cube that formed the starting point of the joint. The cube was then bored out on a lathe to reduce weight and provide recessed bonding ledges for the bi-axial O-ACS. Figure 78 shows the machining process. The bi-axial springs were manufactured with the same geometry and material as those tested in Section 5.3. Plastic compression caps were machined to provide an attachment point for the winching rope

and symmetric compression force to the spring. The springs were cut to a length of 4 in. and bonded into the central cube with 3M structural epoxy DP420.

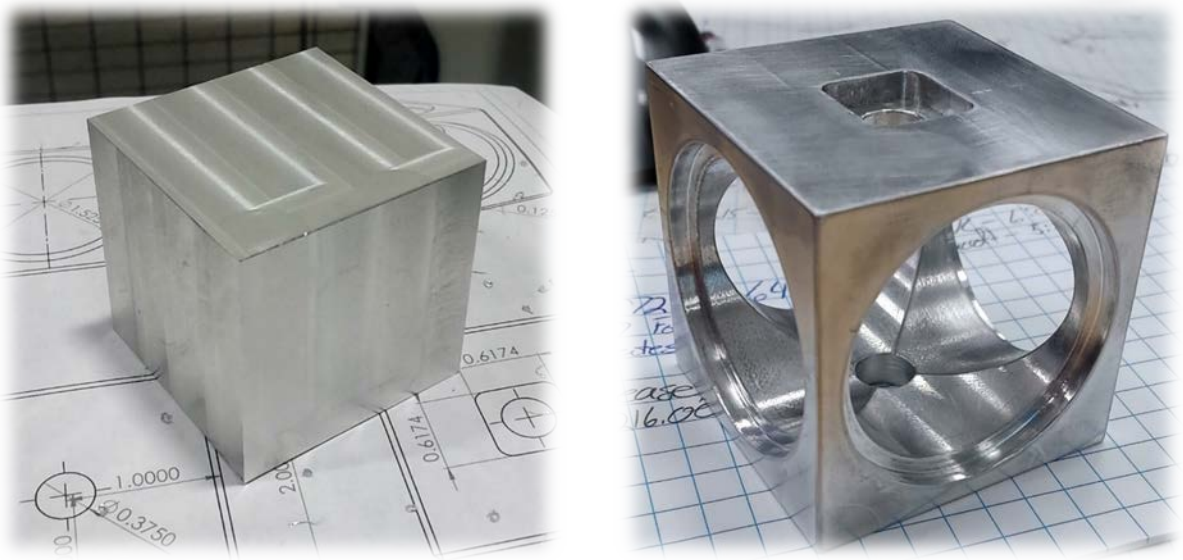

Figure 78 – Central Cube Machining Processes

The rope was braided on a 12 carrier Ratera braiding machine using 6 Kevlar clockwise braiders and 6 nylon braiders to create a strong and lightweight rope. The rope was threaded through the bolt and compression cap and knotted on both ends to provide a simple, reliable, and lightweight mechanism to compress and expand the springs. The finished 4-way joint is seen in Figure 79 through Figure 81.

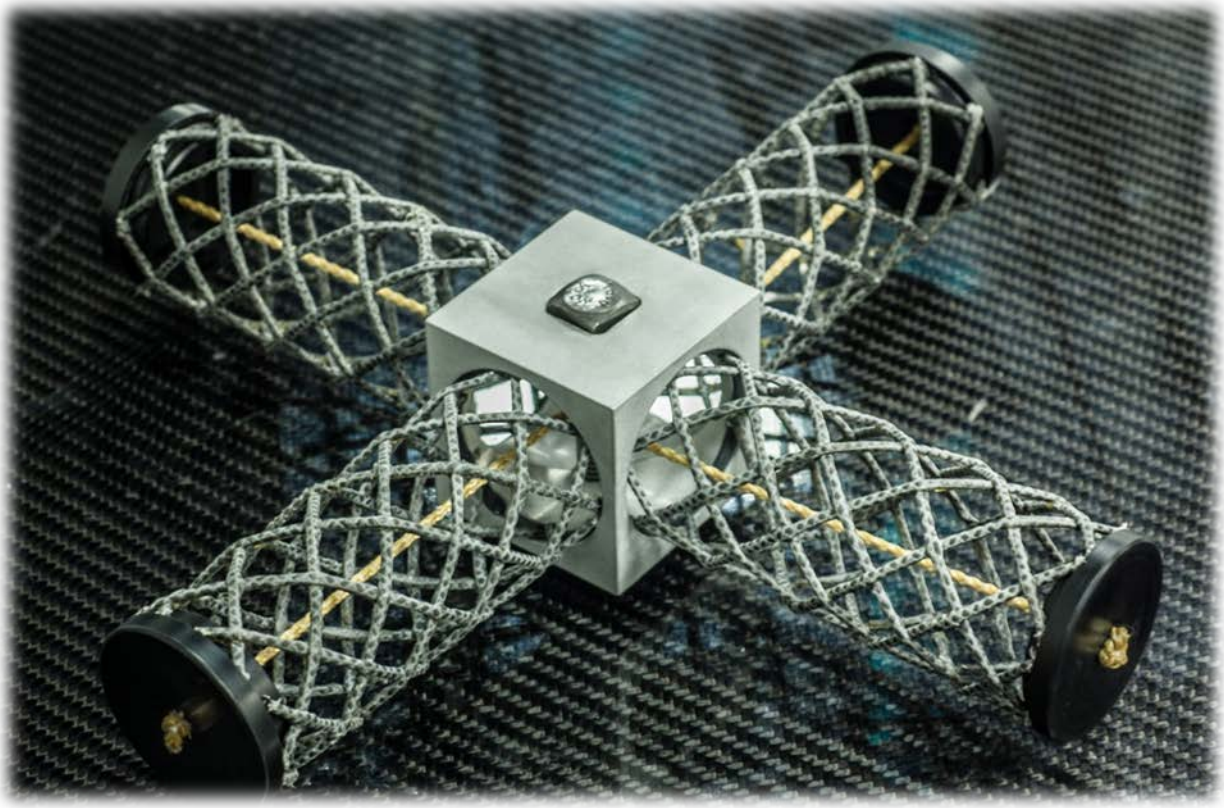

Figure 79 – 4-way Bi-Axial Spring Joint

Figure 80 – 4-Way Bi-Axial Spring Joint in 90° Configuration

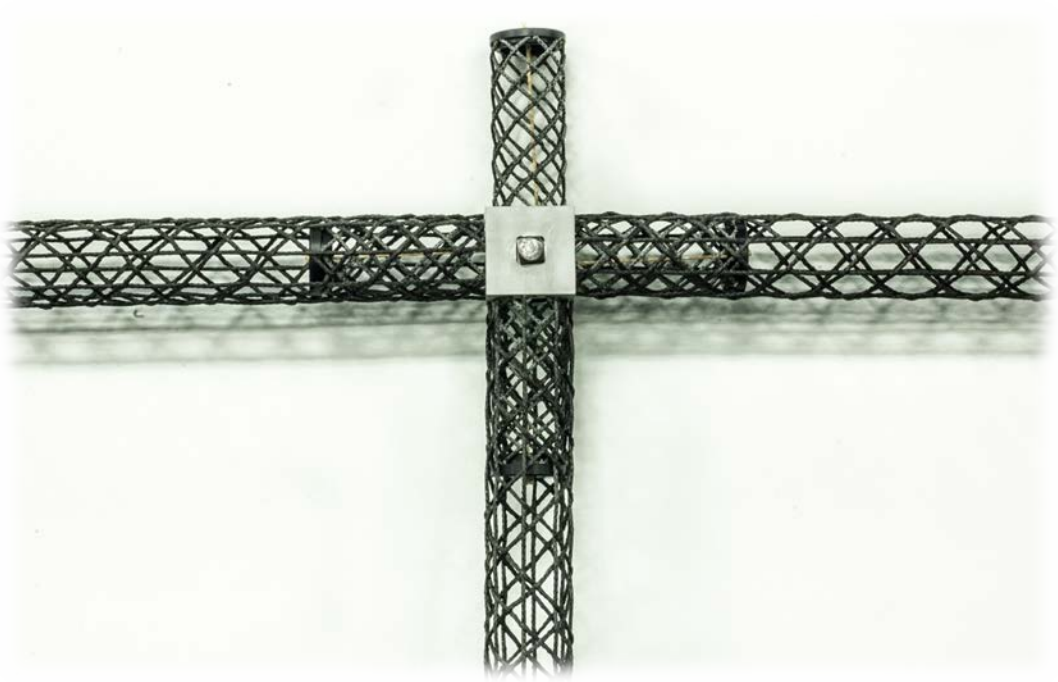

Figure 81 – 4-Way Bi-Axial Spring Joint in 3-way Configuration

Section 5.6 – Future Work on Compressed Bi-Axial Joint

Due to the wide range of parameters that can influence this joining concept, there is no shortage of methods to improve this joint. Three main areas of evolution have been identified: bi-axial spring geometry, cord-preg material, and spring/O-ACS interfacial region.

Owing to the relative lack of understanding on the mechanics of the bi-axial spring, the effects of structure geometry on the spring constant and Poisson's ratio is not well understood. While surface area plays a large role in the performance of this joint, the amount the spring expands and the force required to do so are also important factors. By altering the braid angle of the structure these factors can be manipulated. Adding additional braider cord-preg (6x6 vs. 12x12 structure) will increase surface area and thus friction, but may have an undesirable effect on Poisson's ratio.

The cord-preg used to manufacture these test specimens (cord-preg #22, see Appendix) was chosen based on material availability. However, it is a relatively smooth and round cord-preg due to the jacket materials. This may be beneficial in that it may decrease the compressive force required to expand the spring. Conversely, a rougher cord-preg, such as #6 (see Appendix), may provide higher frictional forces and result in a stronger joint.

The primary mechanism that the joint relies upon is the friction between the O-ACS member and the bi-axial spring. While O-ACS generally have very minimal surface areas, methods of substantially increasing surface areas are suggested. Rubberized coatings on the surface of the bi-axial spring could serve to increase the friction coefficient of the cord-preg material. An interfacial material could also be inserted between the two structures to increase contact area. This material must not constrain the expansion on the spring under compression. A flexible polymeric sheet has been proposed.

The proposed methods of strengthening the compressed spring joint are favored over other possible approaches due to the minimal mass that is added. By altering the geometry, cord-preg or enhancing the interfacial region; a substantial strength increase maybe achieved through a trivial addition of mass. Mass can also be reduced by selecting a lighter weight material for the end caps and central cube of the 4-way joint, such as glass reinforced nylon. As stated above, the design criteria for this joint calls for the O-ACS that are being joined to be unmodified. As such, any improvements to this joint must be made to the bi-axial spring and compression assembly.

Section 5.7 – Conclusions from Evaluation of Compressed Bi-Axial Spring Joint

In this chapter a novel method of temporarily joining unmodified O-ACS members quickly and simply was designed and tested. The objectives of this joint were rapid assembly and disassembly of O-ACS that were, with the exception of being cut to length, unmodified. By

forgoing any sort of mechanical interlocking or secondary bonding, implementing the joint is greatly simplified and requires minimal tools and time. This type of joint is ideal for rapid installation in the field. As trade-off for these functions, strength has been compromised. Test data in Section 5.3 reveals the extent of this trade-off. However, Section 5.6 details possible methods of greatly improving joint strength without adding mass. As research of bi-axial O-ACS advances, a bi-axial spring may be optimized for this application. This type of joint is ideal for lightweight structures that do not endure high loads. One such application that may benefit from this joint would be a lightweight tent structure that could be quickly assembled in the field.

Chapter 6 – Conclusions

Several joints were designed, manufactured, and tested. Data from the testing was evaluated and methods of optimizing the various designs were discussed. Each joining method has advantages and disadvantages, therefore design requirements will govern what joint type is best suited for a given scenario. The joints evaluated in this work were designed for use with the standardized O-ACS and its associated strength characteristics. For O-ACS of significantly higher strength, other joining methods may need to be investigated. An overview of the various joints and pertinent findings follows.

Section 6.1 – Summary of Bonded Metal Joint Findings

Bonded metal joints are versatile and simple, though they lack an emphasis on weight savings. A wide variety of connecting mechanisms can be incorporated in this design, allowing for a family of joints to be produced such that an end consumer could select the needed designs for the given application. Large scale manufacturing of these joints could be done by CNC machining, metal casting, or injection molding; depending on material and the working loads. The simplicity and manufacturing methods of this design also drives manufacturing costs down. The most critical element of this joint may be the selection of the adhesive and determining the optimal length of bonding area for the O-ACS. As seen in Table 12, these metallic joints weighed approximately 0.15 lb., a considerable mass given the minimal mass of the O-ACS. As a result, this joint exceeds when design requirements include simplicity, low price point, and ability to disassemble, but do not necessitate absolute weight savings.

Section 6.2 – Summary of Composite Joint with Metal Insert Findings

The composite nature of this joint provides minimal mass while retaining high strength characteristics. The metallic insert provides a hard-point on the O-ACS that can be used to attach a wide variety of attachment features via threads. Screw threads are universally accepted as a versatile and reliable method of connection. By utilizing a carbon fiber composite material, mass in kept to a minimum; these joints ranged from 0.06 lb. to 0.1 lb. The lay-up of the composite can be tailored to provide the desired mechanical properties without adding extraneous weight. Several methods of manufacture were investigated. Filament winding provides relatively quick and low cost method of manufacture. Hand lay-up provides a very low cost option with a moderate production rate. Over-braiding provides a superior joint but suffers high cost and low production rates. An investigation of methods of integrating the metal insert show the importance of pairing the manufacturing process with a complimentary insert design, as well as the utility of additional adhesive. The tapered shape of the joint minimizes the typical abrupt and brittle failure of composite materials. A composite joint with an integral metal insert provides a lightweight and strong joint that offers a wide range of connecting methods.

Section 6.3 – Summary of Permanently Bonded Joint Findings

Permanently bonded joints are desirable in certain applications where disassembly is unneeded or unacceptable. These joints can be low cost and rapidly manufactured, while remaining simple and providing a high level of strength. Mass also remains low, in the range of 0.01 to 0.05 lb. Adhesive bonding is a widely accepted method of joining load bearing structures that reduces mass and provides a more efficient transfer of load. Many viable adhesives are available to suit the given loading scenario. It was also demonstrated that proper surface

preparation is key to sustaining high loads. Using the lessons learned from the prototype splice and coupler joints, a family of various joint geometries can be manufactured. The coupler joint demonstrated the merits of fully enclosing the O-ACS. A composite material is ideal for minimizing mass if cost is not of concern. A fiber reinforced thermoplastic may suffice given lower loads and an emphasis on lower cost. This joining method achieves a balance of strength, weight, and cost when disassembly is unnecessary.

Section 6.4 – Summary of Compressed Bi-Axial Spring Joint Findings

The joints formed by the compression of bi-axial O-ACS springs are a novel joint design that shows promise for field deployable structures. The design benefits from the use of the bi-axial spring by maintaining the 'openness' of the structure and reducing weight. Its simple operation and ability to rapidly assemble/disassemble may be useful in certain design scenarios. As demonstrated by the testing, this joint is relatively ineffective at sustaining any substantial structural loading. Design alterations have been suggested to improve joint strength. Further research of bi-axial O-ACS may present new methods of improving this design concept. Overall, this concept presents an intriguing method of joining O-ACS members to form temporary and lightweight assemblies.

References

[1] N. Kothari, "Mechanical Characterization of the Braided Composite Yarn and Bond Strength Evaluation of the Joints of the Open-Architecture Composite Structure (O-ACS)," Auburn University, Auburn, 2014.

[2] R. Broughton, D. Branscomb and D. Beale.United States Patent 8859088B2, 2014.

[3] D. Branscomb, "Minimal Weight Composites Utilizing Advanced Manufacturing Techniques," Auburn University, Auburn, 2012.

[4] S. Shirgaonkar, "Development of Test Methods for Evaluation of Bending Stiffness and Compressive Modulus of Braided Composite Lattice Structures," Auburn University, Auburn, 2014.

[5] A. Gurley, "Design and Analysis of Optimal Braided Composite Lattice Structures," Auburn University, Auburn, 2014.

[6] Y. Shen, "Design, Processing, and Failure Analysis of Open-Architecture Composite Structures," Auburn University, Auburn, 2015.

[7] D. McCune, "Manufacturing Quality of Carbon/Epoxy IsoTruss Reinforced Concrete Structures," Brigham Young University, Provo, 2005.

[8] S. Hansen, "Influence of Consolidation and IInterweaving on Compression Behavior of Isotruss Structures," Brigham Young University, Provo, 2004.

[9] D. K. Darooka and D. W. Jensen, "Advanced Space Structure Concepts and their Development," in *AIAA Applied Aerodynamice Conference*, Seattle, 2001.

[10] D. Jegley, K. Chauncey Wu, J. Phelps, M. McKenney, L. Oremont and A. Barnard, "Evaluation of Long Composite Struts," NASA, Hampton, VA, 2011.

[11] M. Ali, F. Fan, P. Khakina and M. H, "Cost-Effective Design of Space Structures Joints: A Review," *International Journal of Civil, Environmental, Structural, Construction and Architectural Engineering*, vol. 7, no. 1, pp. 21-25, 2013.

[12] MERO Tek, "MERO Vision," 2013. [Online]. Available: http://www.mero.de/images/pdf/Vision43.pdf. [Accessed 12 November 2015].

[13] S. Stephan, J. Sánchez-Alvarez and K. Knebel, "Reticulated Structures on Free-Form Surfaces," MERO GmbH & Co, Würzburg, Germany.

[14] P. P. Krimbalis, D. Djokic, G. Hay and R. Cole, "Design and Validation of the Primary Structure and Bonded Joints for the Next Generation Large Canadarm Test Bed," in *Internantional Conference on Composite Materials*, Montreal, 2013.

[15] T. Uozumi and A. Kita, "Carbon Fibre-reinforced Plastic Truss Structures for Satellite using Braiding/Resin Trasfer Moulding Process," *Journal of Materials Design and Applications*, vol. 221, pp. 93-101, 1 April 2007.

[16] Y. H. Q. Z. F. L. F. L. a. Y. G. Dongdong Zhang, "Structural Performance of a Hybrid FRP-Aluminum Modular Triangular Truss System Subjected to Various Loading Conditions," *The Scientific World Journal*, vol. 2014, pp. 1-13, 2014.

[17] 3M, "3M Scotch-Weld Epoxy Adhesive DP460," 2004.

Appendix

Standardized O-ACS

Due to the nearly limitless possibilities for O-ACS geometry and cord-preg material, it was deemed necessary to establish a 'standard O-ACS' for the purposes of this research. All design and testing pertinent to this thesis was conducted in respect to joining O-ACS members of this standardized design. As such, strength properties, dimensions, and possible applications of this particular O-ACS were used as a basis when designing and testing the following concepts. While other designs may be applicable to various other O-ACS geometries, the designs in the thesis are limited to the below described O-ACS. O-ACS members to be joined will henceforth be referred to as standard O-ACS or simply O-ACS in this thesis. The geometry and materials of the standard O-ACS are summarized in Table 9. The cord-preg used in the manufacture of a standard O-ACS is cord-preg #6 (referred to as yarn #6 in some research [1]). Cord-preg #6 is detailed in the following appendix.

Table 9 – Standard O-ACS Geometry

	Quantity	Material
Clockwise Braiders	4	Cord-Preg #6
Counter-Clockwise Braiders	4	Cord-Preg #6
Axials	8	Cord-Preg #6
Braid Angle	45°	
Mandrel Diameter	1.75 in.	

A standard O-ACS has the following true tri-axial braiding geometry: 4 clockwise braiders, 4 counter-clockwise braiders, and 8 axials. The O-ACS is manufactured on a mandrel with a diameter of 1.75 in. and has a braid angle of 45°. All standard O-ACS manufactured for this research were braided on a 64 carrier Wardwell composite braiding machine. Figure 82 shows a section of standard O-ACS.

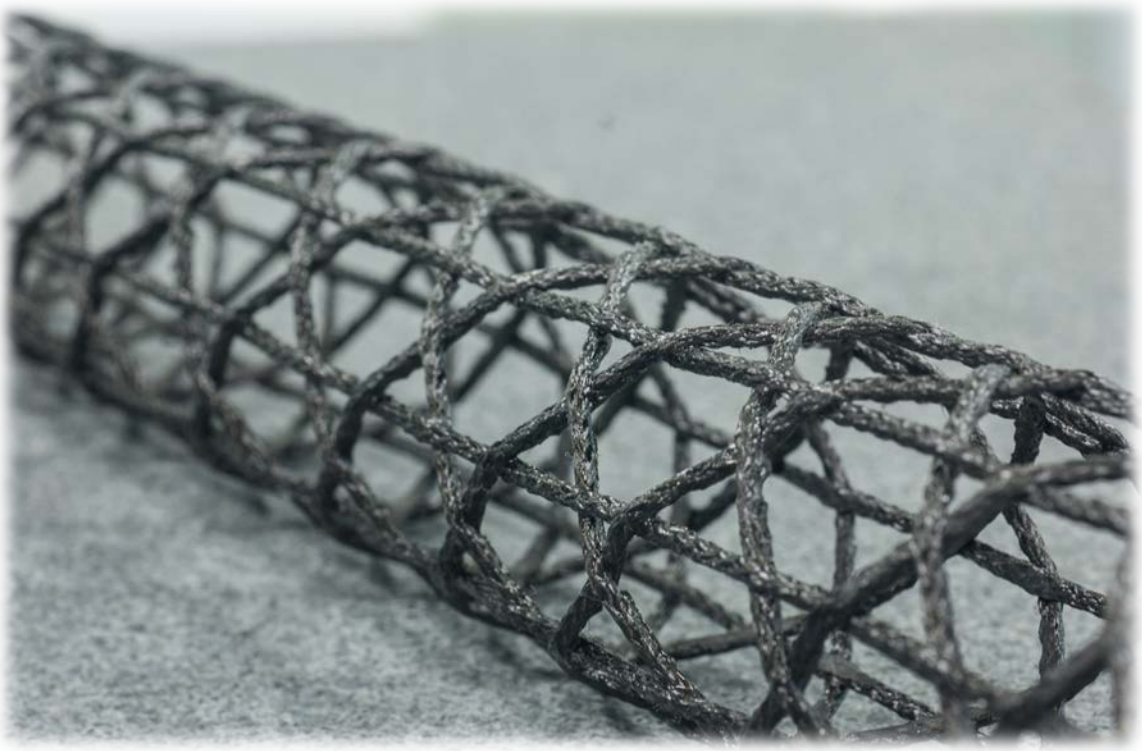

Figure 82 – Standardized O-ACS

Cord-Preg Classifications

Cord-Preg refers to the braided yarn-like structure that is used to braid O-ACS. It is pre-impregnated with a resin system to allow for curing directly after formation. Typically, cord-preg consists of a core that is encapsulated by a jacket. The core contains the majority of the fiber reinforcement that provides the desired material properties. The core is most commonly composed of pre-impregnated carbon fiber tows, ranging from 24k to 120k. Other materials, such as thermoplastics or expanded foams, may be inserted into the core to alter the cross-sectional area or shape. The jacket serves to compact and maintain the shape of the core during subsequent braiding and forming operations. The jacket is typically a true triaxial geometry, often consisting of 8 braiders and 4 axials. Braiding fibers are generally a type of thermoplastic polymer of low denier, such as nylon or polypropylene. Axial fibers may be the same as the

braiders, or may also be a pre-impregnated fiber. The resin system for all cord-pregs manufactured to date has been UF3330, a low-tack resin for braiding.

The cord-preg is manufactured on a traditional braiding machine, typically a 16 or 32 carrier machine. The jacketing yarns are wound onto bobbins and placed accordingly on the carriers and axial positions. The core is fed through the center of the machine to the braiding point under constant tension. The cord-preg then continues onto the take-up machine, consisting of a capstan and re-winding device to transfer the material onto a spool.

Prior O-ACS research has investigated the mechanical properties of varying cord-preg materials. As such, there are numerous cord-preg designations that have been referenced in previous research by Kothari and Shen. The following tables detail the cord-preg used in this thesis. One cord-preg, referred to as “Yarn #6” [1], has been referred to as cord-preg #6 in this thesis.

Figure 83 – Detail View of Cord-Preg #6

Table 10 – Cord-Preg #6 Architecture

	Quantity	Material
Clockwise Braiders	4	500 Denier Textured Nylon
Counter-Clockwise Braiders	4	500 Denier Textured Nylon
Axials	4	3K T300 Carbon Fiber Tow-Preg
Core Material	4	12K (Total 48K) T700 Carbon Fiber Tow-Preg
Braid Angle	45°	

Table 11 – Cord-Preg #22 Architecture

	Quantity	Material
Clockwise Braiders	4	200 Denier Vectran©
Counter-Clockwise Braiders	4	200 Denier Vectran©
Axials	4	200 Denier Vectran©
Core Material	5	12K (Total 60K) T700 Carbon Fiber Tow-Preg
Braid Angle	45°	

Table 12 – Weight of Joints

Joint	Weight (lb)
Metallic Single Clevis	0.1532
Metallic Double Clevis	0.1684
V-Groove Insert	0.0255
Double Taper-In	0.0196
Double Taper-Out	0.0491
Quad-Taper with Pins	0.0524
Hand Laid-up Joint #1	0.0736
Over-Braided Joint #1	0.0639
Over-Braided Joint #2	0.0915
Over-Braided Joint #3	0.1010
1 inch Splice Joint	0.0165
2 inch Splice Joint	0.0355
3 inch Splice Joint	0.0503
Coupler Joint	0.0591
4-Way Bi-Axial Spring Joint	0.5531